

Earth's Future



RESEARCH ARTICLE

10.1029/2022EF002878

Arctic Ocean Freshwater in CMIP6 Coupled Models

Shizhu Wang^{1,2,3} , Qiang Wang⁴ , Muyin Wang^{5,6}, Gerrit Lohmann^{4,7} , and Fangli Qiao^{1,2,3} 

Special Section:

CMIP6: Trends, Interactions, Evaluation, and Impacts

Key Points:

- No significant improvement were found in the simulation of sea surface salinity and liquid freshwater content from Coupled Model Intercomparison Project phase 5 to CMIP6
- CMIP6 models project a 60% rise in the Arctic total liquid freshwater storage at the end of this century in the SSP5-8.5 scenario
- Future Arctic freshwater sources are runoff, net precipitation, Bering Strait inflow and the Barents Sea Opening inflow (largest to least)

Supporting Information:

Supporting Information may be found in the online version of this article.

Correspondence to:

F. Qiao,
qiaofl@fio.org.cn

Citation:

Wang, S., Wang, Q., Wang, M., Lohmann, G., & Qiao, F. (2022). Arctic Ocean freshwater in CMIP6 coupled models. *Earth's Future*, 10, e2022EF002878. <https://doi.org/10.1029/2022EF002878>

Received 2 MAY 2022
Accepted 29 AUG 2022

¹First Institute of Oceanography, Ministry of Natural Resources, Qingdao, China, ²Laboratory for Regional Oceanography and Numerical Modeling, Pilot National Laboratory for Marine Science and Technology (Qingdao), Qingdao, China, ³Key Laboratory of Marine Science and Numerical Modeling, Ministry of Natural Resources, Qingdao, China, ⁴Alfred-Wegener-Institut Helmholtz-Zentrum für Polar- und Meeresforschung (AWI), Bremerhaven, Germany, ⁵Cooperative Institute for Climate, Ocean, and Ecosystem Studies, University of Washington, Seattle, WA, USA, ⁶Pacific Marine Environmental Laboratory, National Oceanic and Atmospheric Administration, Seattle, WA, USA, ⁷University of Bremen, Bremen, Germany

Abstract In this study we assessed the representation of the sea surface salinity (SSS) and liquid freshwater content (LFWC) of the Arctic Ocean in the historical simulation of 31 CMIP6 models with comparison to 39 Coupled Model Intercomparison Project phase 5 (CMIP5) models, and investigated the projected changes in Arctic liquid and solid freshwater content and freshwater budget in scenarios with two different shared socioeconomic pathways (SSP2-4.5 and SSP5-8.5). No significant improvement was found in the SSS and LFWC simulation from CMIP5 to CMIP6, given the large model spreads in both CMIP phases. The overestimation of LFWC continues to be a common bias in CMIP6. In the historical simulation, the multi-model mean river runoff, net precipitation, Bering Strait and Barents Sea Opening (BSO) freshwater transports are $2,928 \pm 1,068$, $1,839 \pm 3,424$, $2,538 \pm 1,009$, and -636 ± 553 km³/year, respectively. In the last decade of the 21st century, CMIP6 MMM projects these budget terms to rise to $4,346 \pm 1,484$ km³/year ($3,678 \pm 1,255$ km³/year), $3,866 \pm 2,935$ km³/year ($3,145 \pm 2,651$ km³/year), $2,631 \pm 1,119$ km³/year ($2,649 \pm 1,141$ km³/year) and $1,033 \pm 1,496$ km³/year ($449 \pm 1,222$ km³/year) under SSP5-8.5 (SSP2-4.5). Arctic sea ice is expected to continue declining in the future, and sea ice meltwater flux is likely to decrease to about zero in the mid-21st century under both SSP2-4.5 and SSP5-8.5 scenarios. Liquid freshwater exiting Fram and Davis straits will be higher in the future, and the Fram Strait export will remain larger. The Arctic Ocean is projected to hold a total of $160,300 \pm 62,330$ km³ ($141,590 \pm 50,310$ km³) liquid freshwater under SSP5-8.5 (SSP2-4.5) by 2100, about 60% (40%) more than its historical climatology.

Plain Language Summary The Arctic Ocean is freshening, rendering strong implications on changes in the Arctic physical and biogeochemical environment. Our knowledge about possible future Arctic changes relies on results from Coupled Model Intercomparison Project (CMIP) models. In this study, we conduct a comprehensive analysis on the Arctic sea surface salinity (SSS), liquid freshwater content (LFWC) and freshwater budget by comparing the new CMIP6 to the previous Coupled Model Intercomparison Project phase 5 (CMIP5) results. An improvement can be found in the SSS simulation in CMIP6, but the large inter-model spread in both CMIP phases makes the improvement insignificant. In CMIP6, the Arctic LFWC remains to be overestimated in the historical simulation. A strong freshening trend is projected in the Arctic Ocean, with the freshwater sources from river runoff and net precipitation persistently increasing in a warming climate. The inflow through the BSO is likely to change from an Arctic freshwater sink to a source around 2050. At the end of this century, the total liquid freshwater storage is expected to rise by 60% under the SSP5-8.5 scenario. In contrast to the increasing LFWC, the solid freshwater content in the form of sea ice is projected to continue declining, with projected summer sea ice vanishing around 2050.

1. Introduction

Sitting at the northern end of the global hydrological cycle, the Arctic Ocean is the freshest ocean in the world. Serreze et al. (2006) estimated that this giant pool holds a total of $74,000 \pm 7,400$ km³ liquid freshwater and 10,000 km³ sea ice in 1979–2001. Freshwater is a key ingredient of the climate system in the Arctic region and beyond. It is important in shaping the Arctic biological communities (Carmack et al., 2016) via, for example, changing the supply of nutrients and organic matter to the Arctic Ocean (Holmes et al., 2012; Kipp et al., 2018; Lara et al., 1998). Moreover, the freshwater over a relatively saline layer sets up a strong halocline which offers protection to the floating sea ice from melting when deep convection occurs (Martinson & Steele, 2001; Polyakov

© 2022 The Authors.

This is an open access article under the terms of the [Creative Commons Attribution-NonCommercial License](https://creativecommons.org/licenses/by-nc/4.0/), which permits use, distribution and reproduction in any medium, provided the original work is properly cited and is not used for commercial purposes.

et al., 2018; Rudels et al., 1996; Steele & Boyd, 1998). Due to an increase in the upward ocean heat flux through the halocline and the recent weakening of the halocline stratification (Polyakov et al., 2020), a slowdown in winter sea ice growth has been observed on the Eurasian side of the Arctic Ocean. The low-salinity Arctic water could also potentially enhance upper ocean stratification in the Labrador and Nordic seas after being released to the North Atlantic in both liquid and solid forms, thus inhibiting deep convection therein and weakening the global thermohaline circulation (Condrón & Winsor, 2012; Häkkinen, 1999; Karcher et al., 2005; Thornalley et al., 2018). Therefore, understanding and adequately predicting changes in Arctic freshwater is of crucial importance.

The Arctic Ocean is fed by several liquid freshwater sources including continental runoff discharge, the Bering Strait inflow and surplus precipitation over evaporation. Pan-Arctic rivers collect the freshwater from snow melting and hose it into the shallow Arctic shelf seas. The river runoff is almost salt-free and forms the largest Arctic freshwater source. Daily discharge data from river outlet stations documented an increase rate of 89 km³ per decade for the four largest Arctic-draining rivers in 1980–2009 (Ahmed et al., 2020). A study combining data assimilation and satellite images demonstrated a larger Arctic river drainage acceleration than previously reported (Feng et al., 2021). The Bering Strait inflow is the second largest freshwater provenance due to the relatively low salinity of the Pacific water. Year-round in situ mooring data suggested a rise rate of about 0.01 Sv per year (1 Sv = 10⁶ m³ per second) in the annual mean volume flux through Bering Strait in 1990–2015 (Woodgate, 2018). Net atmospheric input (precipitation minus evaporation, P-E) is also an important freshwater provenance for the Arctic Ocean (Peterson et al., 2006). These freshwater sources are projected to rise in the future. For example, runoff influx is expected to grow from 4,200 ± 420 km³/year in 2000–2010 to 5,500 km³/year by 2100 (Haine et al., 2015) due to a stronger hydrological cycle in a warming climate. Using an ensemble of CCSM4 projections, Vavrus et al. (2012) estimated that the Arctic precipitation would increase by about 40% by 2100.

In the past few decades, sea ice has decreased both in extent (Stroeve & Notz, 2018) and thickness (Belter et al., 2020; Kwok, 2018). Numerical experiments revealed that in the 2000s, about half of the liquid freshwater content (LFWC) rise in the Beaufort Gyre (BG) could be ascribed to sea ice decline (through both the meltwater and modification of ocean surface stress and circulation) caused by atmospheric warming (Wang, Wekerle, Danilov, Koldunov, et al., 2018). Besides thermodynamic processes, sea ice export to lower latitudes is another main process determining the Arctic solid freshwater content (SFWC) and the total freshwater storage. The sea ice export through Fram Strait accounts for more than 90% of the total sea ice export (Haine et al., 2015; Krumpen et al., 2016).

The upper circulation of the Arctic Ocean is dominated by two primary features, the BG and the Transpolar Drift (Armitage et al., 2017). The Transpolar Drift originates from the Russian Arctic shelves, sweeps across the North Pole and exits the Arctic Ocean through Fram Strait. It is a major conveyor driving sea ice and cold fresh surface water flowing from the Arctic Ocean to the North Atlantic region (Pfirman et al., 1997; Proshutinsky & Johnson, 1997; Spall, 2019). The anticyclonic BG is driven by the predominant Beaufort High atmospheric pressure system. The strong Ekman convergence in this region makes the BG the largest freshwater reservoir in the Arctic Ocean (Haine et al., 2015; Proshutinsky et al., 2002, 2019). Consequently, the liquid freshwater in the Arctic Ocean shows an uneven distribution, with more freshwater trapped on the Amerasian side than on the Eurasian side.

The variability of the Arctic atmospheric circulation is capable of influencing the spatial distribution of Arctic liquid freshwater (Giles et al., 2012; Niederdrenk et al., 2016; Timmermans et al., 2011). Since the mid-1990s when a more anticyclonic atmospheric circulation regime started to become dominant, a concurrent LFWC increase in the Arctic Ocean has been detected from both observations and numerical simulations (Rabe et al., 2014; Wang, Wekerle, et al., 2019). In episodes of increased Arctic Oscillation index, instead of entering the Arctic basin near the Lomonosov Ridge, the Siberian runoff would reroute eastward and enter the Arctic basin through the Makarov Basin (Morison et al., 2012). This shift in the runoff pathway was caused by the change in the LFWC spatial distribution in response to the positive Arctic Oscillation (Wang, Danilov, et al., 2021). Sea ice advecting out of the Arctic Ocean through Fram Strait would also increase under conditions of high Arctic Oscillation index (Rigor et al., 2002), resulting in an Arctic SFWC decrease. It was found that an increase (decrease) in the proportion of water masses of the Atlantic (Pacific) water origin can significantly reduce LFWC regionally, especially in the Eurasian Basin (Wang, Wekerle, et al., 2019). Other factors like sea ice state (S. Wang et al., 2021) and ice-ocean stress feedbacks (Dewey et al., 2018; Meneghello et al., 2018; Spall, 2020; Wang, Marshall, et al., 2019) can also strongly influence the basin-wide LFWC distribution.

The liquid freshwater in the Arctic Ocean has kept rising for decades. The Arctic LFWC was around 93,000 km³ for 1980–2000, but increased to 101,000 km³ in 2000–2010 (Baffin Bay included, Haine et al., 2015). Using salinity data of multiple origins, Rabe et al. (2014) found a positive LFWC trend of 600 ± 300 km³ per year (1992–2012) in the central Arctic basin. The BG LFWC has also shown an increasing trend although it leveled off over some years during the first half of the 2010s (J. Zhang et al., 2016). Based on measurements using multiple observation techniques, Proshutinsky et al. (2019) estimated that the BG LFWC increased by more than 6,400 km³ from 2003 to 2018.

Unlike the increasing LFWC, the Arctic SFWC has a negative trend in the last few decades. The total sea ice volume loss was about 600 km³ per decade in 1901–1940, but it rose to 3,810 km³ per decade in the period 1978–2007 (Schweiger et al., 2019). Satellite records have shown a declining sea ice volume in both summer and winter (Kwok, 2018). These decreasing trends are also evident in numerical simulations forced by atmospheric reanalysis fields (Q. Wang et al., 2016a).

The Arctic SFWC (i.e., sea ice) started to show anthropogenic signals decades ago (S. Min et al., 2008). Notz and Stroeve (2016) found a linear relationship between observed sea-ice loss and cumulative CO₂ emissions. The Arctic LFWC changes significantly on seasonal to decadal time scales in response to wind variability (Cornish et al., 2020; Dukhovskoy et al., 2004; Proshutinsky et al., 2002), but the recent changes in Arctic liquid freshwater budget might already contain signals of anthropogenic climate change (Jahn & Laiho, 2020).

Arctic freshwater content and freshwater budget show large biases in model simulations, which is not only the case for coupled climate models (Khosravi et al., 2022; Shu et al., 2015, 2018, 2020; SIMIP Community, 2020; Zanowski et al., 2021), but also for forced ocean-ice models (Jahn et al., 2012; Q. Wang et al., 2016a, 2016b). Large uncertainties in simulations could influence the prediction and understanding of the changes in the Arctic Ocean. In the Coupled Model Intercomparison Project phase 5 (CMIP5) models, a strong freshening trend in the Arctic Ocean in the future warming climate was projected, while there are large model spreads in the simulated future changes in Arctic LFWC and different liquid freshwater budget terms (Shu et al., 2018). Compared to observations, CMIP5 models underestimate the volume of Arctic sea ice (Shu et al., 2015) and hence the SFWC. Is there a step change in the performance of the new CMIP6 models in simulating the Arctic freshwater content and freshwater budget compared to the CMIP5 models? In this study, we conducted an extensive assessment of Arctic freshwater content and freshwater budget simulated by CMIP6 models with comparisons to observations and CMIP5 models' results. We will focus on the following questions: (a) Did CMIP6 models on average better reproduce observations in their historical simulations? (b) Are the simulated future changes in CMIP6 models similar to those simulated in CMIP5 models? (c) Are the model spreads reduced in CMIP6 models compared to CMIP5 models?

The model data and analysis methods used in this study are given in Section 2, which is followed by model assessment and future projection results in Section 3. Discussions and conclusions are given in Sections 4 and 5, respectively.

2. Materials and Methods

2.1. CMIP Data and Observations

In the CMIP6 protocol, the historical simulation spans the period 1850–2014 (Eyring et al., 2016). For climate projections, the Scenario Model Intercomparison Project (ScenarioMIP; O'Neill et al., 2016) is proposed to use forcings representing different future pathways of societal development, the Shared Socioeconomic Pathways (SSPs). In this study, the monthly outputs from the historical and two ScenarioMIP runs (SSP2-4.5 and SSP5-8.5) of 31 CMIP6 models were employed. Evaluations on CMIP6 models have shown that global warming will continue and scenarios with higher greenhouse gas emission correspond to stronger warming (Fan et al., 2020; Tokarska et al., 2020).

Different model groups provided different number of ensemble realizations. We took the first ensemble member for each model except CESM2. Model information is shown in Table S1 in Supporting Information S1. Most of the models have a nominal horizontal resolution of 1°, except for CNRM-CM6-1-HR and GFDL-CM4 models, which have higher resolution at about a quarter degree ($1,442 \times 1,050$ and $1,440 \times 1,080$, respectively). In the vertical, CMIP6 models generally have more than 40 ocean layers. We also used the historical simulation outputs of 39 CMIP5 models (Table S2 in Supporting Information S1) for directly comparing the performance in representing sea surface salinity (SSS) and LFWC between the two CMIP phases.

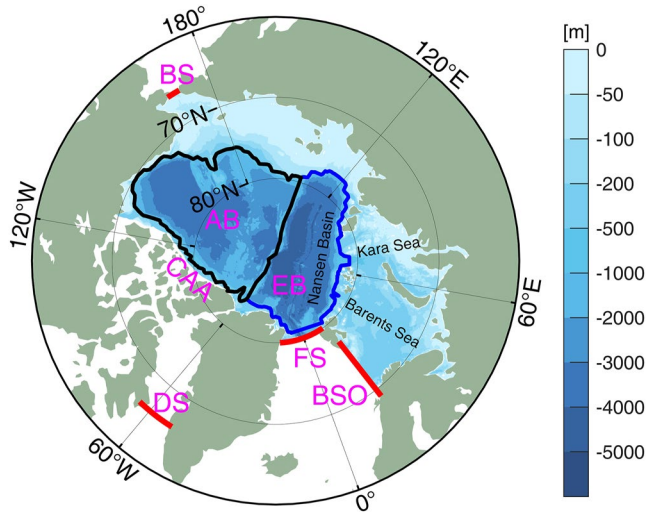


Figure 1. Arctic Ocean bottom topography (unit: m) from ETOPO1 (Amante & Eakins, 2009) inside the Arctic domain. The four Arctic gateways are shown with red lines. The black line encompasses the Amerasian Basin and the blue line the Eurasian Basin. AB: Amerasian Basin; BS: Bering Strait; BSO: the Barents Sea Opening; CAA: Canadian Arctic Archipelago; DS: Davis Strait; EB: Eurasian Basin; FS: Fram Strait.

We use the annual mean climatology of PHC3.0 (Steele et al., 2001) and ORAS5 (Zuo et al., 2019) to assess the model performance in reproducing the Arctic Ocean SSS and LFWC. PHC3.0 is a merged product of WOA (World Ocean Atlas) and AOA (Arctic Ocean Atlas), both of which are based on interpolated in-situ observational data collected mainly from 1950s to 2000s. The time mean over 1950–2005 of the historical run is taken as the simulated climatology by CMIP models and compared to PHC3.0. Observation-based volume and freshwater transports through Arctic gateways (Figure 1) including Fram Strait, Davis Strait, Bering Strait and the Barents Sea Opening (BSO) are also used for model assessment. Sea ice thickness data generated by the Pan-Arctic Ice Ocean Modeling and Assimilation System (PIOMAS; Zhang & Rothrock, 2003) is employed to evaluate the Arctic sea ice volume simulated by CMIP6 models. Other volume and freshwater transport observations and reanalysis data set (e.g., Dee et al., 2011) are also referenced for model-data comparison. All analyses were carried out using annual mean data unless otherwise stated.

2.2. Methods

We stick to the same definition of LFWC as used in previous studies (e.g., Aagaard & Carmack, 1989; Proshutinsky et al., 2019; Shu et al., 2018; Woodgate, 2018). The LFWC is defined as the volume of zero-salinity water per unit area required to be taken out from the ocean so that the salinity of the water column is changed to the chosen reference salinity (Q . Wang et al., 2016b). At each location LFWC is calculated as

$$\text{LFWC} = \int_D^0 (S_{\text{ref}} - S_w) / S_{\text{ref}} dz$$

where S_w is water salinity, $S_{\text{ref}} = 34.8$ psu is the reference salinity and D is the isohaline depth for $S_w = S_{\text{ref}}$ (or the ocean bottom depth if salinity in the whole column is lower than S_{ref}). The total volumetric LFWC in the Arctic Ocean is obtained by integrating over the Arctic Ocean.

The total SFWC is defined as

$$\text{SFWC} = \iint_A \frac{S_{\text{ref}} - S_i}{S_{\text{ref}}} \frac{\rho_i}{\rho_w} h_i ds$$

where $S_i = 4$ psu is sea ice salinity, $\rho_i = 910 \text{ kg m}^{-3}$ is sea ice density, $\rho_w = 1,024 \text{ kg m}^{-3}$ is ocean water density and h_i is the sea-ice volume per grid-cell area (which is also called equivalent sea-ice thickness). For models that do not provide the h_i variable, we multiply sea ice concentration with sea ice thickness to calculate it. Taking all these values into the above equation, we can estimate the SFWC as

$$\text{SFWC} = \iint_A \frac{S_{\text{ref}} - S_i}{S_{\text{ref}}} \frac{\rho_i}{\rho_w} h_i ds \approx 0.79 \iint_A h_i ds$$

which is consistent with other publications (e.g., C. Min et al., 2021; Spreen et al., 2020).

We define the volume transport of ocean water through Arctic gateways as

$$V_{\text{ocean}} = \iint_{\sigma} u_w d\sigma$$

where σ is gateway transect area and u_w is sea water velocity perpendicular to the transect.

The volume transport of liquid freshwater through each gateway is calculated as

$$V_{\text{liquid}} = \iint_{\sigma} u_w (1 - S_w / S_{\text{ref}}) d\sigma$$

and the volume transport of solid freshwater is

$$V_{\text{solid}} = \iint_L \frac{S_{\text{ref}} - S_i}{S_{\text{ref}}} \frac{\rho_i}{\rho_w} h_i u_i dL \approx 0.79 \iint_{\sigma} h_i u_i dL$$

where u_i is sea ice velocity perpendicular to the transect and L is the transect length.

We take the four Arctic gateways close to where the straits are the narrowest as suggested by Griffies et al. (2016). As we try to align the transects along the original gridline of each model for an easy calculation of the transports, the locations of the gateway transects might slightly differ among the models. A zigzag line is needed for calculating the BSO transports because there is no gridlines right across the BSO in almost every model. In order to avoid extra uncertainties resulting from horizontal or vertical interpolation, all the calculations are done on the original model grid except for those only providing output on interpolated grids (e.g., INM-CM5-0). Model results are interpolated onto a common 0.2° longitude-latitude grid for calculating the multi-model mean (MMM) of 2D fields.

Following Serreze et al. (2006) and Shu et al. (2018), we define the region confined by Bering Strait, Fram Strait, the BSO and the northern boundary of the Canadian Arctic Archipelago (CAA) as the Arctic Ocean (Figure 1). When analyzing volume and freshwater transports, Davis Strait is taken as the gateway boundary because the narrow CAA straits are treated differently in different models, for example, with different numbers of straits. Note that the values of liquid and SFWC shown in the paper, for both simulations and observations, are for the defined Arctic domain (Figure 1) rather than the whole sea ice-covered region.

3. Results

3.1. SSS and LFWC Evaluation

The Arctic Ocean is a confluence of saline water from the Atlantic and Pacific oceans and freshwater of different sources (Carmack et al., 2016). On the Atlantic side, high-salinity water flows into the Arctic Ocean through two oceanic gateways (the BSO and Fram Strait), and then gradually mixes with low salinity waters on the way circulating around the continental slopes. A high-salinity tongue fading away into the Arctic Ocean can be observed in the Atlantic sector (Figure 2a). The lowest SSS is found near major river mouths in shelf regions due to the freshness of river water. In the BG region, freshwater converged by strong Ekman transports, including river water and Pacific Water, forms a center of low salinity.

The MMM results of both CMIP phases are able to reproduce the basin-scale pattern of PHC3.0 SSS, including the high-salinity tongue in the Atlantic sector and the low salinity in shelf regions (Figures 2b and 2c). Regional SSS biases, however, exist in several places, with the Amerasian Basin and the East Siberian and Kara seas being too saline, and Nansen Basin and the Barents Sea being too fresh (Figures 2d and 2e). The SSS difference pattern - higher salinity on the Pacific side and lower salinity on the Atlantic side - is quite similar to that of CORE-II models (the Coordinated Ocean-ice Reference Experiments phase II, Ilıcak et al., 2016). From CMIP5 to CMIP6, both positive SSS biases in the Amerasian Basin and negative biases in Nansen Basin and the Barents Sea are decreased. In CMIP5, the mean Amerasian SSS bias is 0.72 psu and the mean Eurasian SSS bias is -0.44 psu. These two values fall to 0.62 and -0.34 psu in CMIP6, respectively. But we also need to note that the seemingly decreased SSS biases from CMIP5 to CMIP6 come with large inter-model uncertainties (panels a–b in Figures S1 and S2 in Supporting Information S1) and hence are not statistically significant.

The East Siberian and Kara seas bear large positive SSS biases in both CMIP5 and CMIP6. In these continental shelf areas, the representation of both river discharge and coastal current can influence the local salinity simulation (Münchow et al., 1999; Steele & Ermold, 2004). For example, in the Kara Sea where rivers Yenisei and Ob hose more than 900 km^3 freshwater each year, we detected a negative correlation between SSS and river runoff, especially in summer after the spring freshet (Figure S3 in Supporting Information S1). In another word, lower SSS comes with more river runoff in these areas.

Figure 3 shows the LFWC derived from PHC3.0 and historical simulations of both CMIP phases. Observation shows that the BG has the highest LFWC with a magnitude of more than 20 m (Figure 3a) while there is relatively lower LFWC over the shallow continental shelf regions (Figure 2a). Fournier et al. (2020) suggested that in some Arctic regions SSS is a good proxy of LFWC. For example, the gradually rising LFWC from the Arctic southern boundary in the Atlantic sector to the interior of the Arctic Ocean is well manifested by the extension of the high-salinity tongue (Figures 2a and 3a).

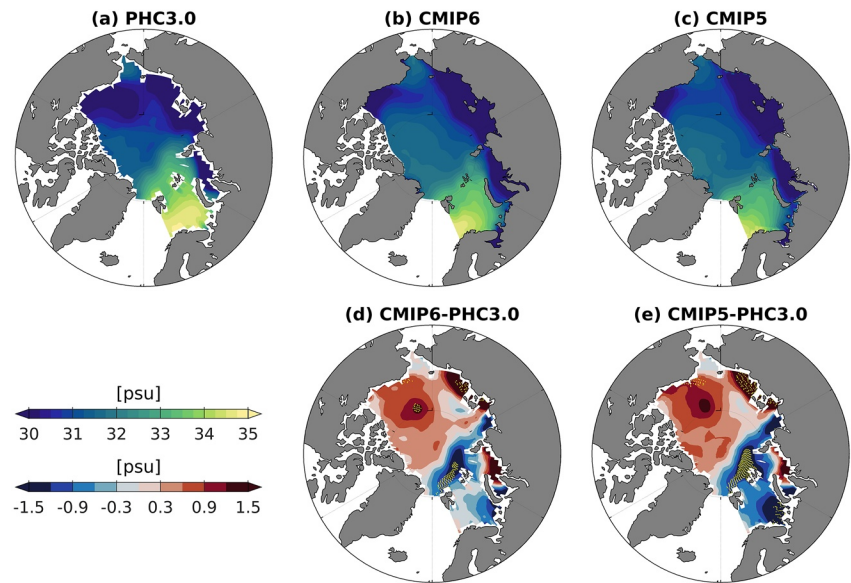


Figure 2. Sea surface salinity (SSS) from (a) PHC3.0 and multi-model means (MMMs) of (b) 31 CMIP6 models and (c) 39 CMIP5 models, and SSS biases of (d) CMIP6 and (e) CMIP5 MMMs relative to PHC3.0. The time mean of historical outputs from 1950 to 2005 is used to represent the SSS climatology of each model. The upper color bar in the bottom left corresponds to salinity shown in panels (a–c), and the lower color bar corresponds to salinity biases in panels (d–e). Magenta scatters in panels (d–e) stand for locations where model-observation bias is larger than inter-model one standard deviation.

The spatial pattern of high LFWC on the Amerasian side and low LFWC on the Eurasian side is captured by both CMIP phases (Figures 3b and 3c). However, both CMIP5 and CMIP6 MMMs overestimate the LFWC (Figures 3d and 3e). The MMMs of both CMIP phases show negative salinity biases in the upper 500 m in the Eurasian Basin (Figure 4a), leading to the overestimated LFWC therein. A giant freshwater pool with LFWC of more than 20 m occupies almost the whole Amerasian Basin, and the concurrence of too high SSS and

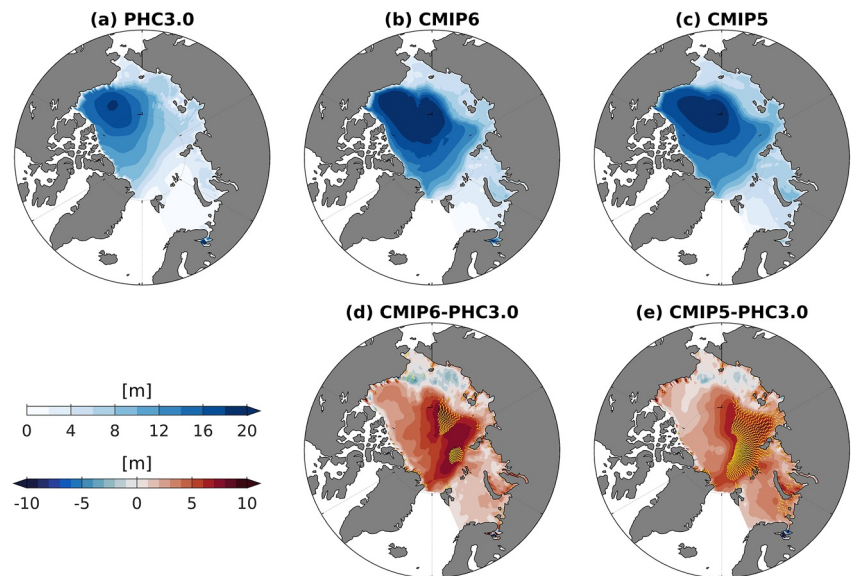


Figure 3. Liquid freshwater content (LFWC) derived from (a) PHC3.0 and MMMs of (b) 31 CMIP6 models and (c) 39 CMIP5 models, and LFWC biases of (d) CMIP6 and (e) CMIP5 MMMs relative to PHC3.0. The LFWC of each individual model is shown in Figures S4 and S5 in Supporting Information S1. The time mean of historical outputs from 1950 to 2005 is used to represent the LFWC climatology of each model. The upper color bar in the bottom left corresponds to LFWC shown in panels (a–c), and the lower color bar corresponds to LFWC biases in panels (d and e). Magenta scatters in panels (d and e) stand for locations where model-observation bias is larger than inter-model one standard deviation.

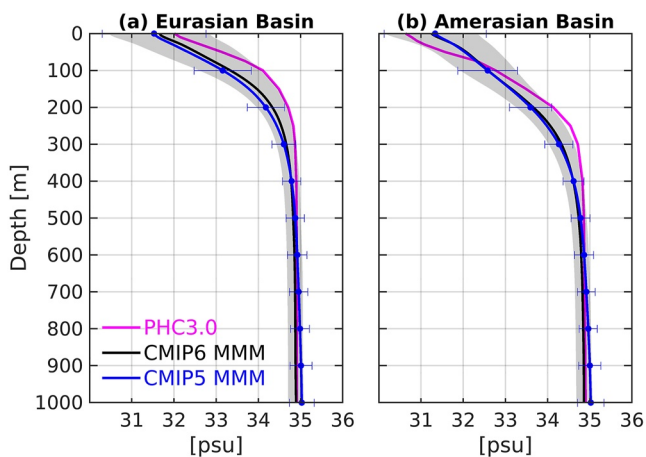


Figure 4. Salinity profiles averaged in the (a) Eurasian Basin and (b) Amerasian Basin from PHC3.0 and the CMIP6 and CMIP5 multi-model means. Shading depicts the range of one standard deviation of CMIP6 results, while CMIP5 one-standard-deviation range is shown by the blue error bars.

excessive freshwater (Figures 2d–2e, and 3d–3e) can be explained by the fact that salinity in the models is overly mixed in the vertical direction, with too high salinity at surface and too low salinity in the mid and lower halocline (Figure 4b). This is consistent with the findings of Khosravi et al. (2022) where they reported negative salinity biases of CMIP6 MMM in the Eurasian Basin while in the Amerasian Basin, the salinity biases are positive in the upper tens of meters and negative in the rest of the water column. Nearly in the whole Amerasian Basin, the modeled LFWC in CMIP6 is more positively biased than in CMIP5 (Figures 3d and 3e). Quantitatively the mean bias in the Amerasian Basin is 4.4 m in CMIP6, while it is 3.2 m in CMIP5. Again, the model-observation bias is less than inter-model LFWC spread (panels c and d in Figures S1 and S2 in Supporting Information S1), especially in CMIP6. The magnitude of the model spreads is similar between CMIP5 and CMIP6, although their spatial patterns are different.

Most CMIP6 models are capable of reproducing the large-scale LFWC pattern: lower in the Eurasian Basin and higher in the Amerasian Basin (Figure S4 in Supporting Information S1, check also the CMIP5 LFWC pattern in Figure S5 in Supporting Information S1). However, other than FGOALS-g3 [No. 17] and INM-CM5-0 [No. 23] which simulate less LFWC compared to PHC3.0, almost all models overestimate the Arctic LFWC, in

both the deep basins and the Arctic Ocean as a whole. Among the models of about 1° horizontal resolution, EC-Earth3 [No. 15] and FIO-ESM-2-0 [No. 18] the most faithfully reproduce the LFWC, resembling the PHC3.0 LFWC in both magnitude and spatial pattern. In order to assess individual model performance and model spread quantitatively, the area-weighted LFWC (in meter) in the Eurasian Basin, the Amerasian Basin and the whole Arctic Ocean are computed (Figure 5). The mean LFWCs of PHC3.0 in these three regions are 6.0, 13.9 and 4.1 m, respectively. As a comparison, the three LFWC values in CMIP6 (CMIP5) MMM are 12.2 m (12.2 m), 18.3 m (17.0 m) and 8.8 m (7.7 m), respectively. All of these basin-wide mean LFWCs are considerably overestimated compared to PHC3.0, for both CMIP5 and CMIP6. More than 1/3 of the CMIP6 models overestimate the freshwater in the Eurasian Basin by more than 100%, and nearly 2/3 of the CMIP6 models overestimate the Arctic mean LFWC by 100%.

3.2. Liquid Freshwater Storage and Fluxes

Observations indicated a LFWC increase in the Amerasian Basin since the mid-1990s while a LFWC decrease in the Eurasian Basin was also recorded (McPhee et al., 2009; Morison et al., 2012; Rabe et al., 2014). The di-pole pattern, a SSS increase and hence LFWC decrease in the Eurasian Basin, and a SSS decrease and hence LFWC increase in the Amerasian Basin, can be well captured by the ORAS5 reanalysis data (Figures 6a and 6e). In the same period, CMIP6 MMM can only simulate the SSS decrease and LFWC increase in the Amerasian Basin but with smaller amplitude (Figures 6b and 6f). The SSS increase and LFWC decrease signal was only confined within the Barents and Kara seas, and did not penetrate to the Eurasian Basin which is evident in ORAS5. The MMM total freshwater stored in the Arctic Ocean is $100,170 \pm 40,120 \text{ km}^3$, which is highly overestimated compared to the $68,490 \text{ km}^3$ freshwater indicated by PHC3.0 (Figures 6g and Table 1). The MMM total freshwater storage starts to increase from the mid-1990s (Figure 6g), which is consistent with the observed liquid freshwater increase (Rabe et al., 2014).

In future warming climates, CMIP6 models project a freshening trend in most parts of the Arctic Ocean, especially along the Arctic coasts (Figures 6c and 6d). In these near-shore regions, SSS is projected to reduce more in a more intense warming scenario, with the sharpest freshening trend being higher than -0.2 psu per decade. Given the negative correlation between SSS and river runoff in these regions (Figure S3 in Supporting Information S1), part of the strong freshening trend can be explained by increasing river runoff in the warming climate (Figure 9a). The signal of rising SSS in the Barents and Kara seas during the historical period is projected to shift to the Eurasian Basin in the future. This is different from CMIP5 results that salinities in both the Eurasian Basin and the Barents and Kara seas are projected to increase in the future (Figure S6 in Supporting Information S1).

Models demonstrate remarkable LFWC increase in future warming scenarios, with more LFWC accumulation along the shelf breaks ($>1.0 \text{ m}$ per decade) while the central Arctic and the Eurasian coastal seas only showing

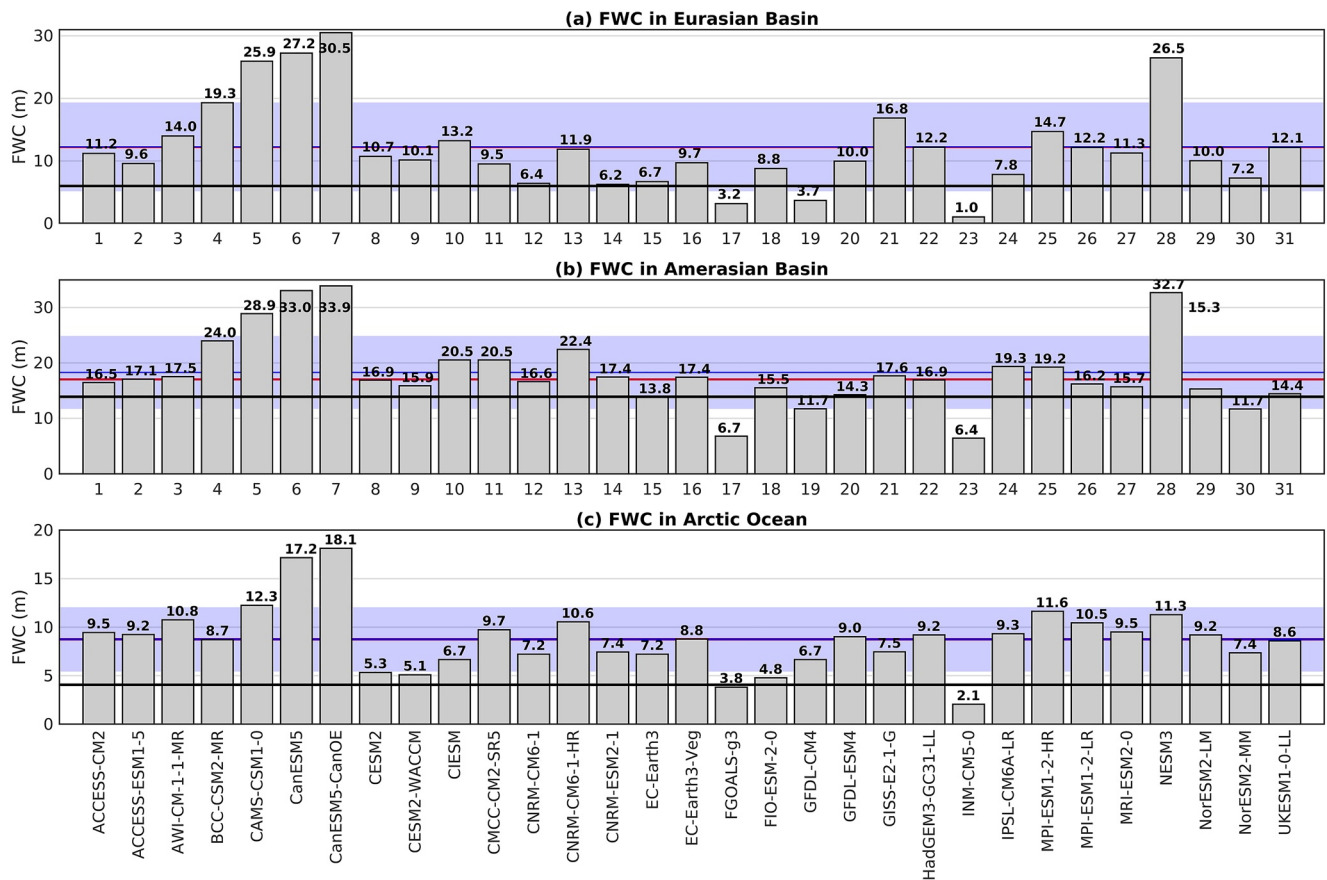


Figure 5. Basin-wide mean liquid freshwater content (LFWC) in the (a) Eurasian Basin, (b) Amerasian Basin and (c) whole Arctic Ocean from CMIP6 models and PHC3.0. The black line marks the LFWC derived from PHC3.0. The blue line is the CMIP6 MMM and the blue shading is MMM \pm one standard deviation (we also call the one-standard-deviation range as inter-model spread or uncertainty in the text). Numbers on x-axes correspond to the model numbers listed in Table S1 in Supporting Information S1. The CMIP5 MMM LFWC (red lines) is also plotted for comparison.

moderate LFWC rise (Figure 6). When forced by rising greenhouse gas concentrations, coupled models show positive trends of the Arctic Oscillation index (Gillett et al., 2002). Q. Wang et al. (2021) found that when the Arctic Oscillation becomes more positive, there is an Ekman transport anomaly directing from the central Arctic Ocean to its periphery, leading to LFWC decrease in central deep basins and LFWC increase in Arctic marginal seas. The significant LFWC rise along the continental slope on the Eurasian side in CMIP6 is absent in CMIP5 (Figure S6 in Supporting Information S1, see also Figure 4 of Shu et al., 2018). The Arctic total freshwater storage remains similar between SSP2-4.5 and SSP5-8.5 till the mid-21st century and the difference becomes obvious afterward (Figure 6i), which is consistent with the projected future evolution of Arctic freshwater budget terms (see Section 3.3 below). By the year of 2100, the Arctic Ocean is projected to hold a total of $160,300 \pm 62,330 \text{ km}^3$ ($141,590 \pm 50,310 \text{ km}^3$) freshwater in the SSP5-8.5 (SSP2-4.5) scenario, about 60% (40%) higher than its historical climatology.

Among the four Arctic gateways, transports through Fram Strait and Davis Strait are major liquid freshwater sinks while the Bering Strait feeds freshwater into the Arctic Ocean. In addition, continental runoff, precipitation minus evaporation (P-E) and meltwater from sea ice are also important liquid freshwater sources for the Arctic Ocean. In the remaining of this section, mean salinities and volume and freshwater fluxes at the Arctic gateways are analyzed.

Pacific water flowing through Bering Strait brings in low-salinity water, contributing to about 30% of the total freshwater into the Arctic Ocean (Serreze et al., 2006). Throughout the historical simulation, CMIP6 MMM captures a net volume transport of about $1.06 \pm 0.43 \text{ Sv}$ (Figure 7a), close to the observation of Roach et al. (1995) in 1990–1994 ($0.8 \pm 0.2 \text{ Sv}$) and Woodgate (2018) in 2003–2015 ($1.0 \pm 0.2 \text{ Sv}$) if the observational uncertainty

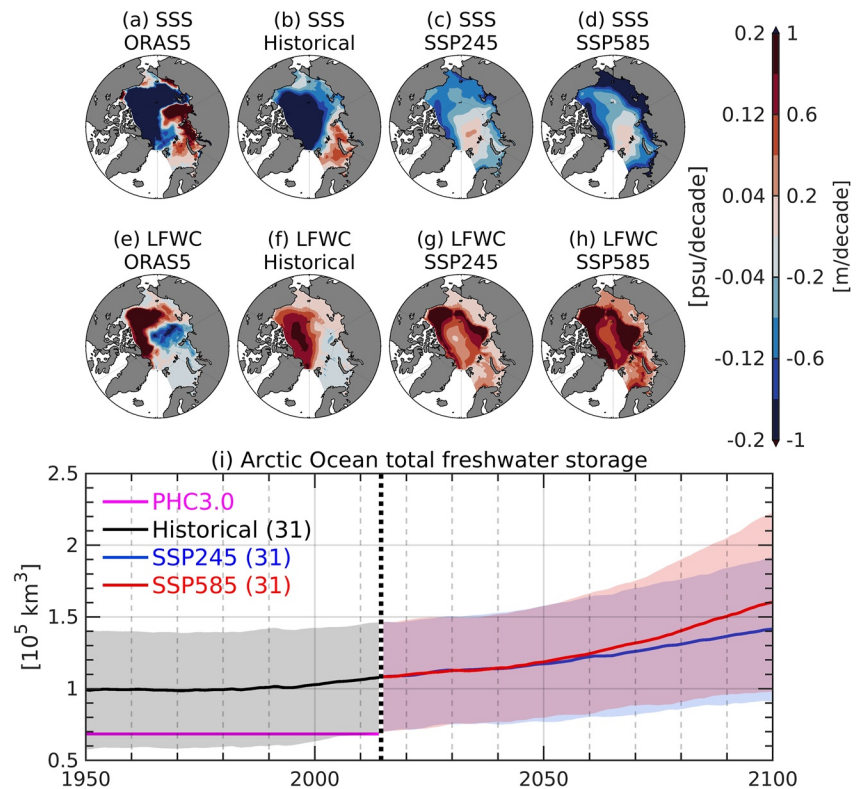


Figure 6. Linear trends of CMIP6 MMM (a–d) sea surface salinity (SSS) and (e–h) liquid freshwater content (LFWC) and (i) the total liquid freshwater storage in the Arctic Ocean. (a, e) ORAS5 trends over 1979–2014, (b, f) CMIP6 historical trends over 1979–2014; (c, g) CMIP6 projected trends over 2015–2100 in the SSP2-4.5 scenario; (d, h) CMIP6 projected trends over 2015–2100 in the SSP5-8.5 scenario. The label on the left side of the color bar corresponds to SSS trend and the right label corresponds to LFWC trend. The number in parenthesis in the legend of (i) means the number of models used in the ensemble analysis. Shading depicts the range of one standard deviation.

Table 1

Annual Mean Arctic Ocean Freshwater Storages (Unit: km^3) and Major Freshwater Budget Terms (Unit: km^3/Year) From CMIP5 and CMIP6 Historical Simulations and Observations

Arctic ocean freshwater budget terms	Observation	CMIP6 mean \pm one standard deviation	CMIP6 (minimum~ maximum)	CMIP5 ^a mean \pm one standard deviation	CMIP5 ^a (minimum ~ maximum)
Liquid storage	68,494 ^b	100,170 \pm 40,120	[34,600~204,950]	103,350 \pm 39,560	[23,510~233,630]
Bering S. (liquid)	2,890 \pm 324 ^c	2652 \pm 1,042	[413~4,484]	1,892 \pm 1,041	[442~4,131]
The BSO (liquid)	-95 \pm 95 ^d	-681 \pm 576	[-1,748~857]	-473 \pm 536	[-1,734~505]
Fram S. (liquid)	-2,700 \pm 530 ^e	-1,785 \pm 896	[-3,982~352]	-3,185 \pm 1,545	[-5,330~442]
Davis S. (liquid)	-2,933 \pm 324 ^f	-2,679 \pm 1,356	[-5,725~524]	-1,703 \pm 1,545	[-4,257~63]
River runoff	3,200 \pm 110 ^g	2,960 \pm 1,069	[242~4,118]	2,617 \pm 1,135	[126~3,816]
P-E	2,016 \pm 161 ^h	1,953 \pm 3,339	[-9,082~5,060]	2,018 \pm 473	[1,293~3,374]
Solid storage	15,964 \pm 1,997 ⁱ	14,688 \pm 1,742	[373~26,317]	—	—
	8,035 \pm 2,548 ^j	7,211 \pm 1,953	[0~19,290]	—	—
Fram S. (solid)	-1,569 \pm 458 ^k -1,904 \pm 504 ^l	-1,407 \pm 174	[-2,788~0]	-1,671 \pm 946	[-4,604~631]
Davis S. (solid)	-331 \pm 45 ^l	-403 \pm 175	[-635~0]	—	—

^aThe freshwater budget terms in CMIP5 are from Shu et al. (2018). ^bderived from PHC3.0. ^cWoodgate (2018), 2000 ~ 2004. ^dHaine et al. (2015), 1980 ~ 2000. ^eHaine et al. (2015), 1980 ~ 2000. ^fCurry et al. (2014), 2004 ~ 2009. ^gSerreze et al. (2006), 1980 ~ 1999. ^hERA-Interim, 1979 ~ 2014. ⁱPIOMAS in March 1979 ~ 2014. ^jPIOMAS in September 1979 ~ 2014. ^kSpreen et al. (2020), 1992 ~ 2013, derived from NSIDC ice drift. ^lSpreen et al. (2020), 1993 ~ 2013, derived from JPL ice drift.

is considered. Similarly, the MMM of CORE-II models reproduce a net volume flux of 1.04 ± 0.32 Sv (Q. Wang et al., 2016b). The simulated freshwater transport through Bering Strait is $2,652 \pm 1,042$ km³/year (Figure 7c), which exhibits improvement compared to that in CMIP5 ($1,892 \pm 1,041$ km³/year, Shu et al., 2018) and CMIP3 ($2,334 \pm 2,523$ km³/year, Holland et al., 2007).

In the warming climate, the persistent freshening in the Arctic Ocean leads to a halosteric sea level rise (J. Yin et al., 2010). In addition, the ocean mass tends to transferring from deep oceans to shallow shelf oceans (Landerer et al., 2007). As a result, the northern side of Bering Strait will experience a higher dynamic sea level rise than the southern side (Figure 8), rendering a decreasing northward volume transport. On the other hand, the salinity of the throughflow also keeps a declining trend (Figure 7b), with larger decrease occurring in warmer climates. The combined changes of volume transport and salinity make the Bering Strait freshwater transport remain relatively stable (Figure 7c). The projected change in Bering Strait freshwater transport anomalies (Figure S7a in Supporting Information S1) is pretty different from that in CMIP5 which projected a first increasing and then decreasing freshwater flux (Shu et al., 2018).

Both saline Atlantic Water and fresh Norwegian Coast Current enter the Barents Sea through the BSO (Smedsrud et al., 2010). Similar to observations (Skagseth et al., 2008), the climatological mean transport is 2.39 ± 0.97 Sv (1950–2005), close to the observation estimation of 2.0–2.3 Sv (1997–2007, Skagseth et al., 2008; Smedsrud et al., 2010, 2013). As a comparison, the MMM net volume flux in CORE-II models is 2.72 ± 0.87 Sv (Q. Wang et al., 2016b). As the BSO salinity is higher than 34.8 psu, the reference salinity (Figure 7e), the relatively higher volume influx causes a negative bias in the MMM freshwater flux (-681 ± 576 km³/year in 1980–2000, Figure 7f); the observed freshwater transport is only about -95 ± 95 km³/year in 1980–2000 (Haine et al., 2015). During the historical simulation, the simulated freshwater flux shows no significant change despite the rise in volume transport after 1980 (Figures 7d–7f) because the BSO salinity is close to the reference salinity.

In different warming scenarios, on average, CMIP6 MMM barely simulates significant trends in the BSO volume transport. The salinity in the BSO, however, keeps decreasing throughout the 21st century (Figure 7e), as a consequence of both the reduction in salt transport from low to high latitudes (due to reduction in AMOC in the warming climate, Collins et al., 2013) and the enhanced water cycle in a warming climate (Vavrus et al., 2012). From 2014 to 2100, the mean salinity in the BSO falls from 35.0 to 34.4 psu (34.6 psu) in the SSP585 (SSP245) scenario. Around 2040–2050, the mean salinity is projected to fall below the reference salinity (34.8 psu), making the BSO inflow shift from an Arctic freshwater sink to a source. CMIP6 MMM projects a steady rise in the BSO freshwater transport in the future (Figure 7f). This is different from CMIP5 MMM in which the BSO freshwater transport will rise slowly before an abrupt increase after 2040. In CMIP5 results, the future change of the BSO freshwater flux exhibits the largest inter-model spread among all the Arctic freshwater budget terms. In CMIP6 the model spread is reduced considerably (Figure S7b in Supporting Information S1) and is smaller than some other budget terms.

As the only deep connection between the Arctic Ocean and the world ocean, Fram Strait is a confluence of several water masses (e.g., Stöven et al., 2016) and is a major freshwater sink for the Arctic Ocean. Main ocean currents include northward West Spitsbergen Current and southward East Greenland Current. Observations show a net volume flux of about -2.0 ± 2.7 Sv in 1997–2006 (Schauer et al., 2008), and the CMIP6 MMM (-2.46 ± 1.26 Sv) stays within the large observation uncertainty in the same period (Figure 7g). The estimated net freshwater flux through Fram Strait by Haine et al. (2015) is $-2,700 \pm 530$ km³/year in 1980–2000. In contrast to the overestimation in CMIP5 ($-3,185 \pm 1,545$ km³/year, Shu et al., 2018) and CMIP3 ($-3,090 \pm 3,090$ km³/year, Holland et al., 2007), CMIP6 MMM ($-1,785 \pm 896$ km³/year) underestimates the climatological freshwater throughflow (Figure 7i).

The net freshwater flux of Fram Strait is projected to continue the rising trend of the historical simulation until around 2060, after which the intensity of the freshwater transport will stay relatively stable in both scenarios. Before 2060, both the volume transport increase (Figure 7g) and salinity decrease (Figure 7h) contribute to the rising freshwater outflow. In the last few decades of the 21st century, volume transport starts to fall and offsets the effect of decreasing salinity, causing a relative stable freshwater outflow (Figure 7i). Compared to CMIP6, CMIP5 MMM projected a weaker increase in Fram Strait freshwater flux (Figure 6 in Shu et al., 2018). The leveling off of the freshwater transport simulated by CMIP6 models is absent in CMIP5 results.

Separating the inflow and outflow enables to quantify their individual contribution to the net transport through the strait. Over the last two decades the Atlantic inflow increased and caused a warming trend in the Arctic

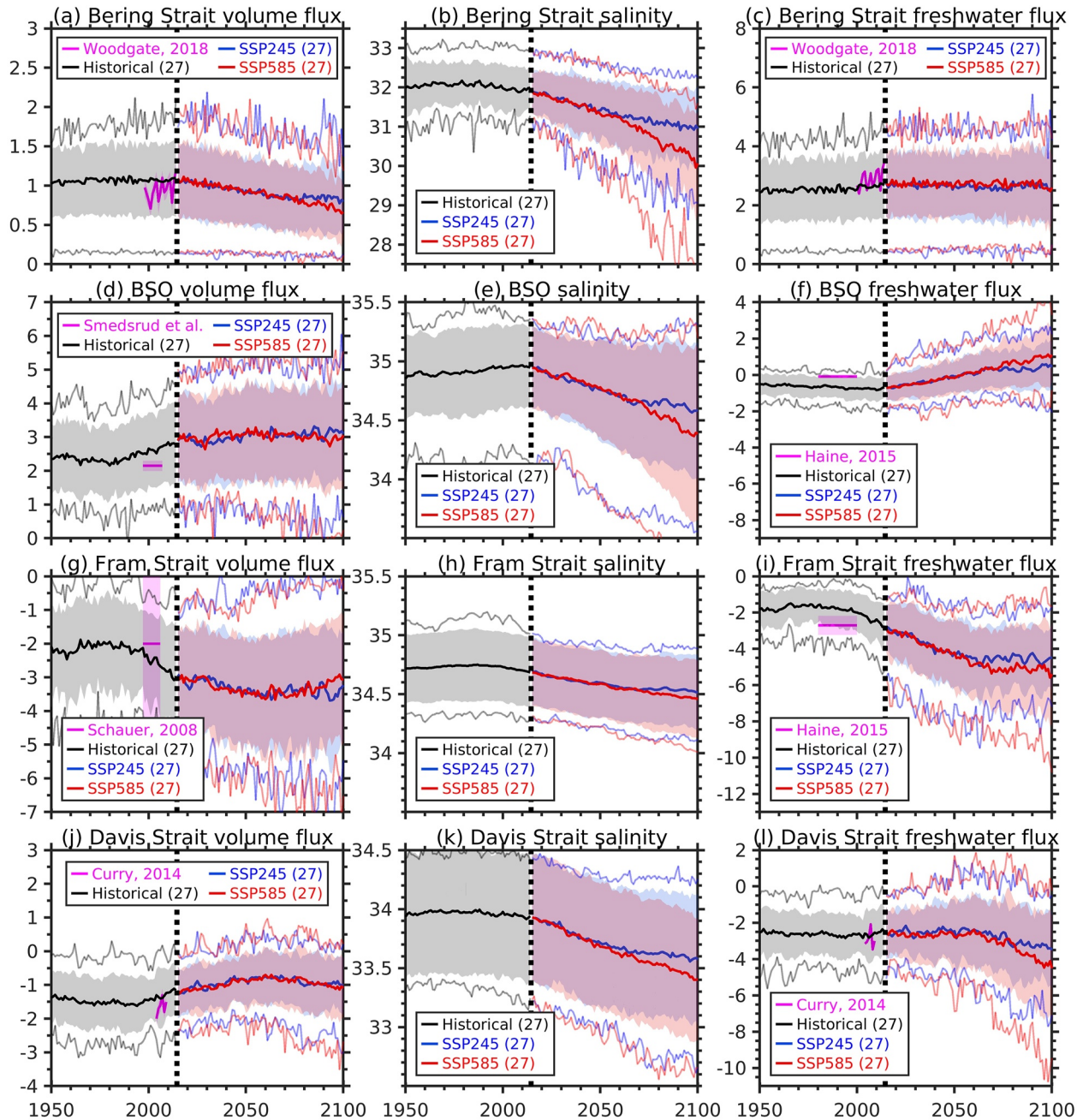


Figure 7. CMIP6 multi-model mean (left column) net volume flux, (middle column) area-weighted salinity and (right column) net freshwater flux for (a–c) Bering Strait, (d–f) the Barents Sea Opening, (g–i) Fram Strait and (j–l) Davis Strait. Units of volume flux, salinity and freshwater flux are Sv, psu and $10^3 \times \text{km}^3/\text{year}$, respectively. The dashed line in each panel denotes the demarcation between historical simulation and future projection. In the left and right columns, positive indicates net flow into the Arctic Ocean while negative stands for outflow. The thin lines depict the 5th and 95th percentiles of the model ensemble, and shading shows the range of one standard deviation. The number in parenthesis in the legend of each panel means the number of models used in the MMM calculation. Available observations are also provided for model-observation comparison. Note the difference of y-axis ranges between Bering Strait (3 Sv, 6 psu, $8 \times 10^3 \text{ km}^3$) and the other three gateways (8 Sv, 2 psu, $13 \times 10^3 \text{ km}^3$). Check also the simulated and observed freshwater budget terms in Table 1. In panel (d), we combine estimations from Smedsrud et al. (2010), Skagseth et al. (2008) and Smedsrud et al. (2013) together to give an observation estimation of the Barents Sea Opening (BSO) net volume transport as 2.0–2.3 Sv.

Atlantic Water layer (Q. Wang et al., 2020). The CMIP6 models consistently simulated an increase in Atlantic Water import through Fram Strait in the early 21st century (Figure S8 in Supporting Information S1). However, after about 2020, the Atlantic inflow does not change a lot until the end of the 21st century. Overall, the change in the net volume transport largely follows the change in the outflow, and the net freshwater transport is also mainly

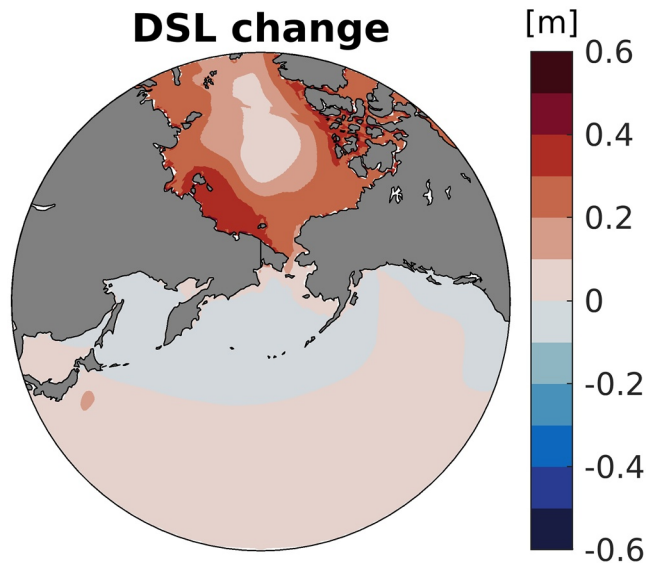


Figure 8. CMIP6 multi-model mean dynamic sea level change in 2018–2100 (SSP5-8.5) relative to 1995–2014.

dominated by the freshwater outflow. Because the salinity in the Atlantic Water inflow has a decreasing trend in the 21st century, after about 2040 the inflow will become a small freshwater source for the Arctic Ocean in the SSP5-8.5 scenario.

Davis Strait is another volume and freshwater sink for the Arctic Ocean. Freshwater passes through the CAA into Baffin Bay and then leaves Davis Strait as the surface-intensified Baffin Island Current (Cuny et al., 2005). On the eastern side of Baffin Bay, West Greenland Current brings relatively salty and warm waters along western Greenland. Moored arrays along the strait section recorded a declining net transport from -2.0 ± 0.5 Sv in 2004–2005 to -1.5 ± 0.5 Sv in 2009–2010 (Curry et al., 2014). The declining volume transport can be reproduced by CMIP6 results (Figure 7j). The net freshwater transport through Davis Strait was observed to be about $-2,933 \pm 324$ km³/year in 2004–2010 (Curry et al., 2014) and it can be well represented by CMIP6 models ($-2,679 \pm 1,356$ km³/year in 2004–2010, Figure 7l).

In future warming scenarios, the mean salinity at Davis Strait shows a persistent falling trend (Figure 7k), with more decline happening in the warmer scenario. The declining volume transport before 2060 counteracts the effect of the falling salinity, and thus causes a relatively stable freshwater flux (Figures 7i). The volume fluxes exporting the Fram and Davis straits show opposing changes (Figures 7g and 7j, Figures S8a and S8d in Supporting

Information S1), which might be attributed to the changing dynamic sea levels in the Arctic Ocean and North Atlantic subpolar gyre (Nummelin et al., 2016; Q. Wang et al., 2022). After 2060, the volume transport has an increasing trend, together with the decreasing trend of salinity, leading to a rise in the net freshwater outflow. The changes in net volume and freshwater transports through Davis Strait are largely determined by the changes in the outflow, that is, the Baffin Island Current (Figure S8f in Supporting Information S1). The projected future evolution of Davis Strait freshwater transport in CMIP6 is very different from that in CMIP5. In CMIP5 the Davis Strait freshwater transport shows a rapid increase when simulations transit from historical to future simulations (Figure 6 of Shu et al., 2018).

River runoff and P-E are two important freshwater provenances for the Arctic Ocean (Serreze et al., 2006). Compared to the CMIP5 result ($2,617 \pm 1,135$ km³/year, Shu et al., 2018), CMIP6 models show improvement in the simulated river runoff in the historical runs ($2,960 \pm 1,069$ km³/year, Figure 9a), in comparison to $3,200 \pm 110$ km³/year in the same period estimated by Serreze et al. (2006). In the scenario simulations river runoff increases, with higher increase in warmer climate. The increase in river runoff is stronger in CMIP6 than in CMIP5 (see CMIP5 results in Figure 1 of Nummelin et al., 2016 and Figure 6 of Shu et al., 2018). In particular, in the SSP5-8.5 scenario, CMIP6 MMM simulates a runoff rise of 1,555 km³/year (Figure S7e in Supporting Information S1) till the end of this century relative to the historical climatology. This result is similar with the findings of Zanowski et al. (2021) who used seven CMIP6 models with more ensemble members and found that runoff is expected to increase from 3,546 km³/year in the historical simulation to 5,605 km³/year in the SSP5-8.5 projection. As a contrast, the projected runoff increase by CMIP5 models is about 946 km³/year (Shu et al., 2018).

The Clausius-Clapeyron equation dictates about a 7%/°C increase in moisture content in the lower troposphere (Held & Soden, 2006). The mid-latitude storm tracks are expected to intensify with poleward and upward shifts (J. H. Yin, 2005), supplying more moisture from low to high latitudes and enhancing precipitation and runoff over the Arctic region in the warming future (Tebaldi et al., 2021; X. Zhang et al., 2013). According to CMIP6 simulations, P-E rises slowly in the historical period, and the MMM flux ($1,953 \pm 3,339$ km³/year) can perfectly reproduce that in the ERA-Interim reanalysis data ($2,016 \pm 161$ km³/year, Figure 9b). On the other hand, the model spread of P-E is the largest among all the freshwater budget terms. Like the response of river runoff to future warming, P-E increases in a warming climate, with a higher increase in the warmer scenario. Compared to CMIP5, the rise in P-E is more pronounced in CMIP6. Indeed, relative to the mean of the 1950s, in CMIP5 the BSO transport and river runoff are the two largest freshwater suppliers to the Arctic Ocean at the end of this century (Shu et al., 2018), while in CMIP6, P-E increases the most and is the largest contributor to Arctic freshening (Figures S7f in Supporting Information S1). From the historical and SSP5-8.5 results, we found a linear

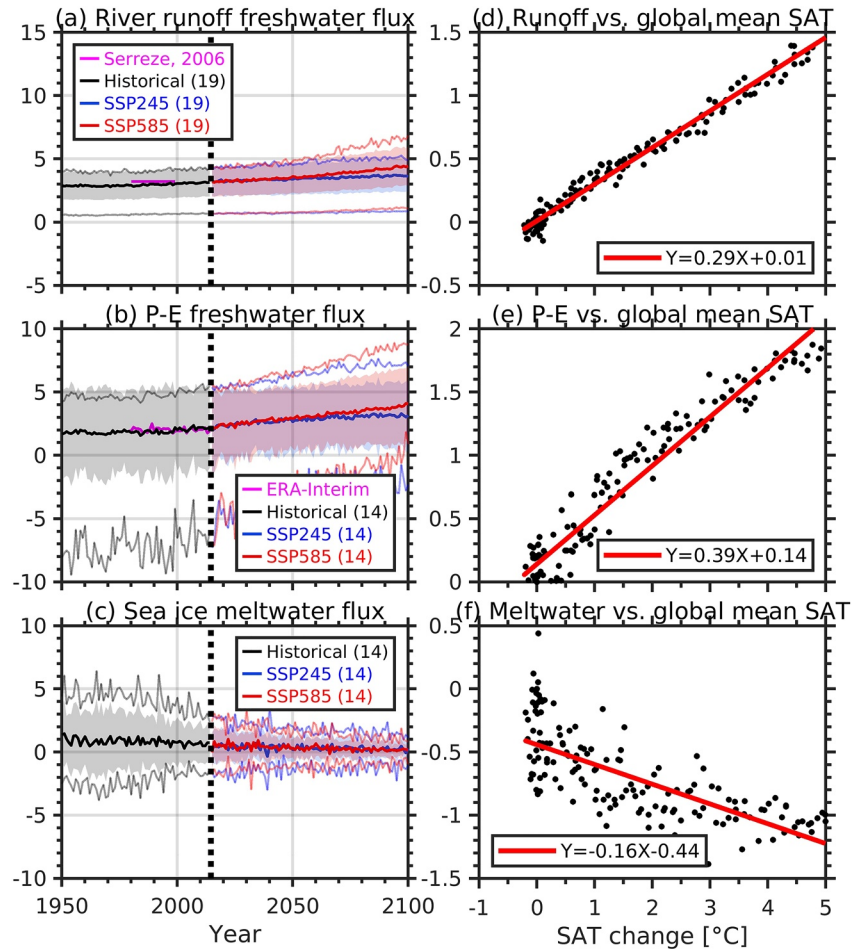


Figure 9. Left column: CMIP6 multi-model mean (MMM) net liquid freshwater flux from (a) river runoff, (b) precipitation minus evaporation (P-E) and (c) sea ice melting (unit: $10^3 \times \text{km}^3/\text{year}$). Right column: MMM freshwater flux changes relative to 1950 within the Arctic Ocean (unit: $10^3 \times \text{km}^3/\text{year}$) versus global mean surface air temperature (SAT) change in the historical simulation and SSP5-8.5 projection. The dashed line in the left column denotes the demarcation between historical simulation and future projection. Positive indicates net flux into the Arctic Ocean while negative stands for outflow. The thin lines depict the 5th and 95th percentiles of the model ensemble, and shading depicts the range of one standard deviation. The number in parenthesis in the legend means the number of models used in the MMM calculation. Available observations are also provided for model-observation comparison. Shown in the plot are annual mean results. Check also the simulated and observed freshwater budget terms in Table 1.

relationship between the strength of the water cycle (runoff, precipitation and evaporation) and the global mean surface air temperature in CMIP6 models, with CMIP6 MMM showing a $280 \text{ km}^3/\text{year}$ and $380 \text{ km}^3/\text{year}$ flux rise per degree of warming for river runoff and P-E, respectively (Figures 9d and 9e).

As the Arctic carries on warming, an ice-free Arctic Ocean in summer seems to be an inevitable situation independent on forcing scenarios applied in CMIP6 models (SIMIP Community, 2020). With the reduction in sea ice volume, sea ice meltwater flux decreases with time in a warming climate (Figure 9c). CMIP6 MMM shows that sea ice meltwater decreases by $160 \text{ km}^3/\text{year}$ for every one degree of global warming (Figure 9f).

The model spreads of the climate change signal (anomaly referenced to the 1950s mean) of Arctic freshwater budget terms are shown in Figure S7 in Supporting Information S1. Despite the very small mean values at the end of the 21st century (Figure 9c), sea ice meltwater has a very large model spread in its climate change signal, similar to those of P-E and freshwater transports through Fram and Davis straits (Figure S7 in Supporting Information S1). The model spreads of climate change signals of river runoff and freshwater transports through Bering Strait and the BSO are relatively smaller. Different from CMIP6 models, the model spread of climate change signals is the largest in the BSO freshwater transport in CMIP5 models (Shu et al., 2018). Model spreads in the freshwater transport through Fram and Davis straits are similar between the two CMIP phases.

3.3. Solid Freshwater Storage and Fluxes

Sea ice is a more general indicator of Arctic warming than other variables. It is reported that CMIP6 MMM and the MMMs of the previous two CMIP phases reproduce similar Arctic sea ice area climatology that is consistent with observations (SIMIP Community, 2020). The MMM of CMIP6 historical runs simulates a rapid SFWC decrease starting from the 1980s (Figures 10a and 10b), with the SFWC in March decreasing from $16,976 \pm 6,993$ in 1980 to $11,863 \pm 3,804$ km³ in 2014, and the SFWC in September decreasing from $9,767 \pm 6,967$ to $4,391 \pm 3,106$ km³. In the same time span, the simulated SFWC by PIOMAS is generally more than CMIP6 MMM but locates well within the large model uncertainty, reducing from 18,607 to 12,247 km³ in March, and from 11,174 to 4,929 km³ in September. Summer sea ice is projected to continue the current declining trend into the future, and disappear around the year 2050 in both emission scenarios considered here. Sea ice in winter also keeps a fast melting in the first half of the 21st century for both scenarios, but an appreciable deceleration emerges in SSP2-4.5 after 2050.

The solid freshwater transports through the four main gateways are projected to keep declining (Figures 10c–10f). This is expected given the persistently retreating sea ice (Figures 10a and 10b), and the fact that the trend of sea ice volume transport is determined by sea ice thickness (Langehaug et al., 2013; Q. Wang, Ricker, et al., 2021). The sea ice inflow through Bering Strait nearly reaches zero around 2060 in both scenarios, but it keeps a multi-decadal variability in SSP2-4.5 afterward (Figure 10c). Sea ice exiting the BSO almost totally disappears around 2050, indicating a sea-ice free Barents Sea in the second half of this century (Figure 10d). In the past several decades, sea ice import into this region declined sharply and enhanced vertical mixing of the water column, making the northern Barents Sea the warming hotspot in the Arctic (Lind et al., 2018).

As the main oceanic gateway of Arctic sea ice export, Fram Strait accounts for about 90% of the total Arctic sea ice outflow (Haine et al., 2015; Serreze et al., 2006). According to the estimation of Spreen et al. (2020), the solid freshwater outflow through Fram Strait has kept decreasing since the 1990s, which can be reproduced by models although models tend to underestimate the decrease rate (Figure 10e). The difference between SSP2-4.5 and SSP5-8.5 starts to emerge from 2040 and keeps growing in the process of the continued warming. The Davis Strait solid freshwater outflow remained stable at first and started to decrease from 1990 onwards. The observation by Curry et al. (2014) indicated a Davis Strait sea ice outflow of -331 ± 45 km³/year in 2004–2010, and CMIP6 MMM reproduces an outflow of -403 ± 175 km³/year in the same time period. When the Davis Strait outflow continues decreasing in the future, scenario-induced difference emerges around 2060, with the outflow almost vanishing in SSP5-8.5 in 2100 but stabilizing around -200 km³/year in SSP2-4.5.

3.4. Total Freshwater Budgets

A freshwater budget analysis is conducted by summing up all the freshwater sources and sinks that have been discussed above as shown in Figure 11. Note that sea ice formation or melt does not change the total freshwater stored in the Arctic Ocean, and should be excluded from the budget analysis. According to the CMIP6 projection in SSP5-8.5, river runoff, net precipitation (P-E) and the Bering Strait inflow will remain the three largest freshwater sources. Unlike the relatively steady Bering Strait inflow, P-E is projected to rise with time and become the second largest freshwater source around 2040. The transport through the BSO (i.e., the BSO inflow) has long been considered as a freshwater sink for the Arctic Ocean (e.g., Haine et al., 2015), but this is projected to change in the second half of the 21st century according to CMIP6 MMM results (see also Figures 10 and 11 in Zanowski et al., 2021). The BSO salinity maintains a declining trend (Figure 7e) and is going to be lower than 34.8 psu, the reference salinity, around 2055, after which the BSO inflow is projected to become a freshwater supplier.

Of all the freshwater sinks, the outflow through Davis Strait remains relatively constant, while the Fram Strait outflow grows persistently and contributes the largest freshwater export after 2010. In the SSP5-8.5 scenario, the total solid freshwater outflow through the four gateways decreases fast and almost vanishes at the end of this century, while in SSP2-4.5, this solid term is projected to decrease before 2060 and remain relatively steady afterward. In the historical period before 1990, a subtle balance was kept between sources and sinks (the black lines in Figure 9). The balance was broken and biased to the source side after 1990, the time perfectly corresponding to when observation started to record a freshening Arctic Ocean (Rabe et al., 2014). The sum of freshwater sources and sinks keeps enlarging in the future warming scenario, leading to an increase of the total liquid freshwater storage in the Arctic Ocean (Figure 6).

We found most CMIP6 models have simulated an overestimated LFWC already in their piControl runs, a reference state that happened more than a century before the recently observed Arctic freshening (Figure S9 in Supporting

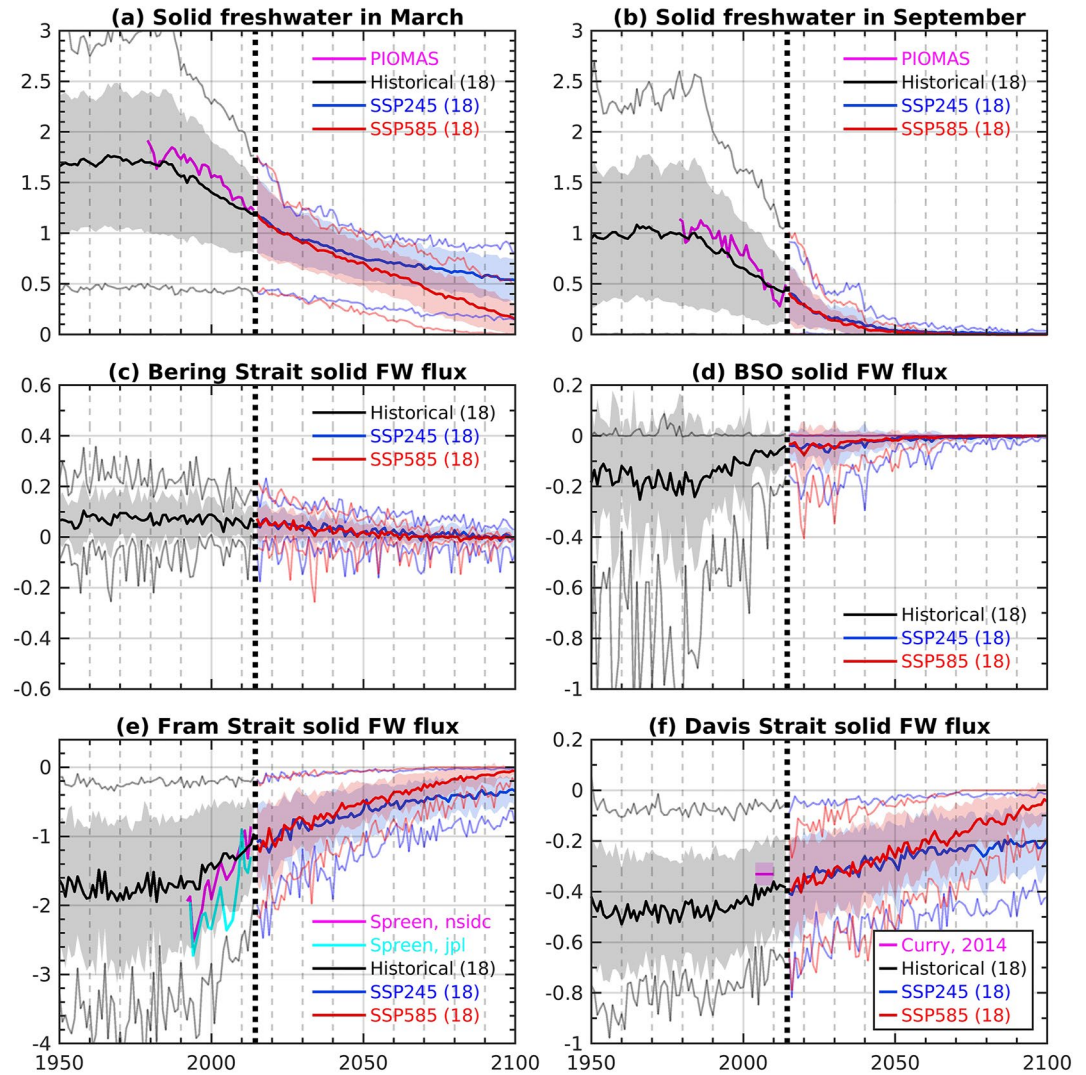


Figure 10. CMIP6 multi-model mean (MMM) solid freshwater storage (unit: $10^4 \times \text{km}^3$) in (a) March and (b) September, and the annual mean solid freshwater flux (unit: $10^3 \times \text{km}^3/\text{year}$) through (c) Bering Strait, (d) the Barents Sea Opening, (e) Fram Strait and (f) Davis Strait. The dashed line in each panel denotes the demarcation between historical simulation and future projection. Positive numbers in panels (c–f) indicate net flux into the Arctic Ocean while negative stands for outflow. Shading depicts the range of one standard deviation. The thin lines depict the 5th and 95th percentiles of the model ensemble. The number in parenthesis in the legend of each panel means the number of models used in the MMM calculation. The PIOMAS data are also provided for model-reanalysis comparison. The values shown in panels (a and b) are values for the Arctic domain shown in Figure 1 and do not represent the whole ice-covered region. Note the difference of y-axis ranges between Fram Strait flux ($4.2 \times 10^3 \text{ km}^3/\text{year}$) and fluxes through the other three gateways ($1.2 \times 10^3 \text{ km}^3/\text{year}$). In panel e, two estimations by Spreen et al. (2020) from different observation data are provided. See more details in their Figure 8.

Information S1). So the overestimated LFWC in the historical period (Figures 3, 5, and 6) was likely inherited from the piControl run state which was caused by model deficiency in representing some important processes. Rosenblum et al. (2021) found that some coupled models tend to simulate an unrealistic vertical mixing in the upper Arctic Ocean and accordingly fail to capture the observed freshwater change in recent years.

4. Discussions

Throughout the analysis, we compared MMM results to observations, and found large inter-model spread in model results. The large model scatter is not specific to coupled climate models but rather exists also in ocean-sea ice models (Ilicak et al., 2016). Three potential error sources could contribute to and thus partly explain these model spreads.

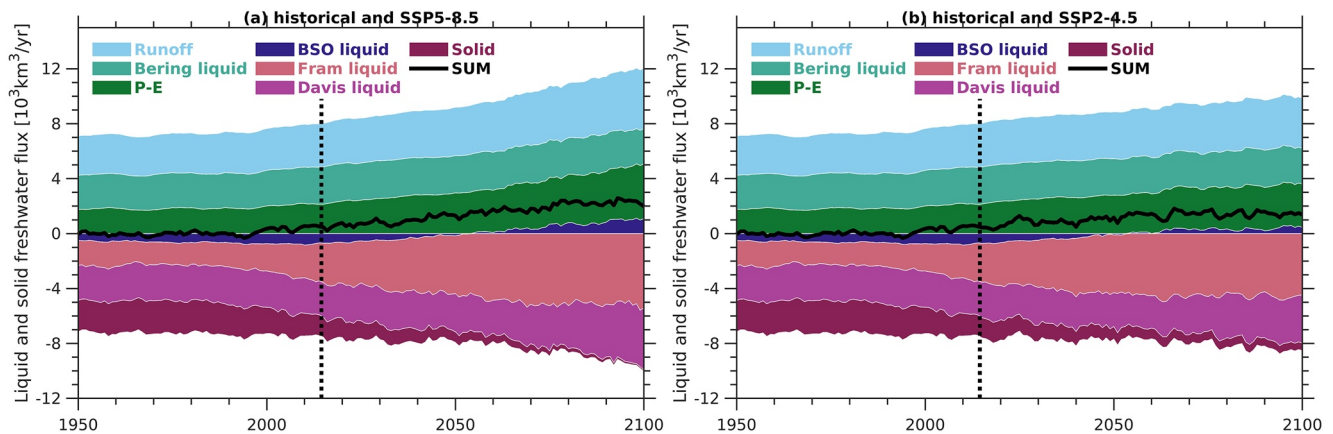


Figure 11. (a) Annual mean freshwater sources and sinks for the Arctic Ocean in 1950–2100 (historical and under scenario SSP5-8.5) from CMIP6 multi-model mean (MMM) results, (b) the same with (a) but for historical and SSP2-4.5. The thickness of each color stripe represents the quantity of that source or sink while the black lines are the sum of all sources and sinks. Solid freshwater transport through the four gateways is shown as a whole. The dashed lines denote the demarcation between the historical simulation and future projection. Positive indicates freshwater flux into the Arctic Ocean while negative stands for outflow.

The first type of uncertainty comes from the fact that we used only one member of realizations from each model, a common practice in the model assessment works (e.g., Held & Soden, 2006; Shu et al., 2018). As observation and simulation should be different realizations of the chaotic climate system, model-observation biases are bound to exist. To prove the validity of using one realization member to represent the model's performance, we conducted a multi-member comparison from three CMIP6 models, and each of them have 7 or more realizations (Figure S10 in Supporting Information S1). We found that for each model, although an intra-model spread does exist in the LFWC simulation among different members, no significant difference exists between the ensemble-member mean and individual members. This means that for each model, the model-observation biases in representing the climatology or long-term mean are largely systematic biases inherent in that model, or internal variability is negligible on a long time scale. The long-term mean of one realization can thus well represent the model's ability in simulating the mean state of Arctic freshwater. Zanowski et al. (2021) also reported that the intra-model spread is smaller than the inter-model spread for both liquid and solid freshwater storage simulation in CMIP6 models. These were also mentioned in a recent study by Khosravi et al. (2022) in that the difference in the simulated mean state in the Arctic Ocean is smaller than the inter-model differences. Noteworthy is that, however, Zanowski et al. (2021) highlighted the importance of internal variability in the estimation of fluxes through, for example, the Barents Sea Opening. For these specific circumstances, it is more appropriate to include more realization members for the assessment of a model's performance. It is also worth noting that although we used more CMIP6 models than Zanowski et al. (2021) and hence some quantities such as the projected runoff discharge at the end of this century might vary from that of Zanowski et al. (2021), major findings of this study, for example, overestimation of the liquid freshwater storage by models and projected freshening of the Arctic Ocean in the future, remain unchanged.

The second type of uncertainty is related to the method that we used for flux calculation. Griffies et al. (2016) suggested that original velocities without interpolation should be used and strait transects should be along the original gridline of each model for flux computation. The grids employed by CMIP6 models are mostly different, and there are always differences in their gridlines and hence the transect locations. To investigate the sensitivity of flux calculation to changing section locations, we computed fluxes through three locations of each Arctic gateway based on two models. We found that changing the transect location could indeed introduce some variations in the calculated flux. The minor difference, however, is trivial compared to inter-model differences (Figure S11 in Supporting Information S1). Spreen et al. (2020) reported a similar finding that the calculation of sea ice volume transport was insensitive to the exact gateway location. This means that the large spreads in the calculated volume and freshwater fluxes shown in Figures 7 and 10 are in large part due to the inter-model differences (Figure 11).

The third type of error resides in the deficiency of CMIP models to physically describe the dynamical processes in the Arctic Ocean. For example, model resolution can impact the spatial pattern of liquid freshwater in the Arctic Ocean (Fuentes-Franco & Koenigk, 2019; Q. Wang, Wekerle, Danilov, Wang, & Jung, 2018). Model uncertainty could be also due to important yet missing processes in the model. For example, it has been demonstrated that tides

are able to enhance ocean mixing (Holloway & Proshutinsky, 2007) and hence the communication between the Atlantic Water with cold and fresh surface waters (Luneva et al., 2015). Interactions between sea ice and waves are also important in shaping the mixing of the upper ocean (Cole et al., 2018; Guthrie et al., 2013). The strength of vertical mixing can significantly influence upper ocean salinity and hence the LFWC (J. Zhang & Steele, 2007). Improvement in the representation of the Arctic salinity is expected if these missing processes can be adequately incorporated into climate models. In addition, the Arctic freshwater budget is also determined by the atmospheric processes and the ocean states in sub-Arctic seas. Therefore, improvements in each component model are required in order to effectively reduce the overall uncertainties in the simulated Arctic freshwater storage and budget.

Uncertainties inherent in the observation and reanalysis datasets could also contribute to model-observation biases. We employed the LFWC derived from PHC3.0 (Steele2001) as the LFWC observation and compared it to CMIP6 results. In the Arctic Ocean, PHC3.0 is a blend of several observation-based data sources and bears its own uncertainty. So far there is no error estimation for this product. In the SFWC assessments, the PIOMAS data was used. Although PIOMAS is physically constrained by observed sea ice concentration the underlying model still suffers from deficiencies as most of the ocean climate models do. Schweiger et al. (2011) reported that the uncertainty of PIOMAS sea ice volume data can be as high as $2,800 \text{ km}^3$.

5. Conclusions

In the current study we assessed Arctic SSS and LFWC in 31 CMIP6 and 39 CMIP5 models. We then compared volume and freshwater fluxes through oceanic gateways and three surface liquid freshwater budget terms (runoff, precipitation minus evaporation, sea ice melting) to observation and/or reanalysis data, and assessed their future changes. An assessment of the SFWC and gateway transports was also performed, after which a total budget analysis involving all freshwater sources and sinks was conducted.

Relative to PHC3.0, the MMM of CMIP6 models more reasonably simulates Arctic SSS than CMIP5 models, with both positive SSS biases in the Amerasian Basin and negative SSS biases in the Eurasian Basin diminishing in CMIP6. On the other hand, CMIP6 models do not show improvement in the representation of LFWC, and it even deteriorates in the Makarov Basin. Given the large model spreads in both CMIP phases, however, the difference in both SSS and LFWC was insignificant between the two phases. Our quantitative analysis shows that almost all CMIP5 and CMIP6 models overestimate the Arctic LFWC, both in the deep basins and averaged over the whole Arctic Ocean.

Future climate warming renders a carry-on Arctic freshening as shown by CMIP6 scenario simulations, with SSS decreasing in most parts of the Arctic Ocean and LFWC generally increasing especially along the continental slope. The amplitudes of the SSS decrease and LFWC increase in CMIP6 are larger than in CMIP5. We also found that CMIP6 models on average have a slight SSS rise in the central Eurasian Basin, while in CMIP5 the center of SSS increase occurs in the Barents Sea. An increase in SSS implies a weakening in upper ocean stratification and strengthening in vertical mixing, which probably presents a signal of Arctic Atlantification (Polyakov et al., 2017) as a result of Arctic sea ice decline (Q. Wang et al., 2020; S. Wang et al., 2021). At the end of the 21st century, the Arctic Ocean is projected to hold a total of $160,300 \pm 62,330 \text{ km}^3$ ($141,590 \pm 50,310 \text{ km}^3$) freshwater in the SSP5-8.5 (SSP2-4.5) scenario, about 60% (40%) higher than the simulated historical climatology.

CMIP6 MMM can reasonably represent volume and freshwater transports through Arctic gateways and freshwater fluxes from river runoff and precipitation minus evaporation (P-E). In the historical simulation, the climatological freshwater net fluxes averaged over 1950–2005 from river runoff, P-E, and Bering Strait are $2,928 \pm 1,068$, $1,839 \pm 3,424$, and $2,538 \pm 1,009 \text{ km}^3/\text{year}$, respectively. All of these freshwater sources will increase in the future warming climate. In the last decade of this century, these values are projected to be $4,346 \pm 1,484 \text{ km}^3/\text{year}$ ($3,678 \pm 1,255 \text{ km}^3/\text{year}$), $3,866 \pm 2,935 \text{ km}^3/\text{year}$ ($3,145 \pm 2,651 \text{ km}^3/\text{year}$) and $2,631 \pm 1,119 \text{ km}^3/\text{year}$ ($2,649 \pm 1,141 \text{ km}^3/\text{year}$) in the SSP5-8.5 (SSP2-4.5) scenario, while sea ice meltwater flux will decrease to about zero around the mid of the 21st century in both scenarios. The BSO is a freshwater sink in the historical simulation ($-636 \pm 553 \text{ km}^3/\text{year}$ in 1950–2005), but it is projected to become a freshwater source due to the persistently declining salinity in the BSO inflow, with the mean value in 2091–2100 rising to $1,033 \pm 1,496 \text{ km}^3/\text{year}$ ($449 \pm 1,222 \text{ km}^3/\text{year}$) in SSP5-8.5 (SSP245). Of the two major freshwater sinks, freshwater export through Davis Strait is projected to stay unchanged before 2060 and become higher afterward. The Fram Strait freshwater export, on the contrary, is expected to increase first and then keep relatively stable afterward, staying to be the largest Arctic freshwater sink at the end of the 21st century.

Large inter-model spreads of SSS and LFWC exist in both CMIP6 and CMIP5 historical simulations, with CMIP6 models exhibiting smaller SSS but larger LFWC spreads. Among all the freshwater budget terms in CMIP6, net precipitation exhibits the largest inter-model spread (one standard deviation is about 3,339 km³/year). For the climate change signals of the Arctic freshwater budget (anomalies relative to the mean of 1950s), the model spread of the BSO freshwater transport in CMIP6 is smaller than in CMIP5, but the spreads of sea ice meltwater and P-E become larger in CMIP6. The model spreads of the climate change signals of Fram and Davis straits freshwater export in CMIP6 remain similarly large as in CMIP5. Over all, no obvious reduction can be found in the inter-model spreads of Arctic freshwater budget climate change signals in CMIP6 compared to CMIP5.

In this study, we discussed freshwater processes including freshwater storage in the Arctic Ocean and fluxes through Arctic gateways. Some freshwater-related processes are still missing in the current CMIP models but are worth mentioning here. The Greenland Ice Sheet melting is an important freshwater supplier but is ruled out by current generation climate models. From 1995 to 2010, the Greenland Ice Sheet drains surface runoff and solid ice with a rate of 77 ± 7 km³/year into the Arctic Ocean (Bamber et al., 2012). The rate of ice sheet mass loss (and hence freshwater input to the ocean) is likely to become even larger in the future and thus exceed the maximum rates of the past 12,000 years (Briner et al., 2020). Incorporating the relevant cryosphere processes into climate models will be necessary for improving simulation results and providing more faithful freshwater-related projections in the future (e.g., Ackermann et al., 2020; Muntjewerf et al., 2020).

Data Availability Statement

All CMIP5 and CMIP6 model simulations are available online (<https://esgf-node.llnl.gov/projects/cmip5/> and <https://esgf-node.llnl.gov/projects/cmip6/>). The PHC3.0 data can be downloaded from http://psc.apl.washington.edu/nonwp_projects/PHC/Climatology.html, and the ORAS5 data is downloaded from <https://www.cen.uni-hamburg.de/en/icdc/data/ocean/easy-init-ocean/ecmwf-oras5.html>. The code for calculating fluxes through oceanic gateways and plotting the figures can be downloaded from <https://zenodo.org/record/6630376#.YycKXZBxdi>.

References

- Aagaard, K., & Carmack, E. C. (1989). The role of sea ice and other fresh water in the Arctic circulation. *Journal of Geophysical Research*, 94(C10), 14485–14498. <https://doi.org/10.1029/jc094ic10p14485>
- Ackermann, L., Danek, C., Gierz, P., & Lohmann, G. (2020). AMOC Recovery in a multicentennial scenario using a coupled atmosphere-ocean-ice sheet model. *Geophysical Research Letters*, 47(16), e2019GL086810. <https://doi.org/10.1029/2019gl086810>
- Ahmed, R., Prowse, T., Dibike, Y., Bonsal, B., & O'Neil, H. (2020). Recent trends in freshwater influx to the Arctic Ocean from four major Arctic-draining rivers. *Water*, 12(4), 1189. <https://doi.org/10.3390/w12041189>
- Amante, C., & Eakins, B. W. (2009). *ETOPO1 arc-minute global relief model: Procedures, data sources and analysis*. NOAA Technical Memorandum NESDIS NGDC-24. National Geophysical Data Center, NOAA. <https://doi.org/10.7289/V5C8276M>
- Armitage, T. W. K., Bacon, S., Ridout, A. L., Petty, A. A., Wolbach, S., & Tsamados, M. (2017). Arctic Ocean surface geostrophic circulation 2003–2014. *The Cryosphere*, 11(4), 1767–1780. <https://doi.org/10.5194/tc-11-1767-2017>
- Bamber, J., van den Broeke, M., Ettema, J., Lenaerts, J., & Rignot, E. (2012). Recent large increases in freshwater fluxes from Greenland into the North Atlantic. *Geophysical Research Letters*, 39(19), L19501. <https://doi.org/10.1029/2012gl052552>
- Belter, H. J., Krumpfen, T., von Albedyll, L., Alekseeva, T. A., Frolov, S. V., Hendricks, S., et al. (2020). Interannual variability in transpolar drift ice thickness and potential impact of Atlantification. *The Cryosphere Discussions*, 1–24.
- Briner, J. P., Cuzzzone, J. K., Badgley, J. A., Young, N. E., Steig, E. J., Morlighem, M., et al. (2020). Rate of mass loss from the Greenland Ice Sheet will exceed Holocene values this century. *Nature*, 586(7827), 70–74. <https://doi.org/10.1038/s41586-020-2742-6>
- Carmack, E. C., Yamamoto-Kawai, M., Haine, T. W. N., Bacon, S., Bluhm, B. A., Lique, C., et al. (2016). Freshwater and its role in the Arctic Marine System: Sources, disposition, storage, export, and physical and biogeochemical consequences in the Arctic and global oceans. *Journal of Geophysical Research G: Biogeosciences*, 121(3), 675–717. <https://doi.org/10.1002/2015JG003140>
- Cole, S. T., Toole, J. M., Luc, R., & Lee, C. M. (2018). Internal waves in the Arctic: Influence of ice concentration, ice roughness, and surface layer stratification. *Journal of Geophysical Research: Oceans*, 123(8), 5571–5586. <https://doi.org/10.1029/2018jc014096>
- Collins, M., Knutti, R., Arblaster, J., Dufresne, J.-L., Fichefet, T., Friedlingstein, P., et al. (2013). Long-term climate change: Projections, commitments and irreversibility. In *Climate change 2013—the physical science basis: Contribution of working group I to the Fifth assessment report of the intergovernmental panel on climate change* (pp. 1029–1136). Cambridge University Press.
- Condron, A., & Winsor, P. (2012). Meltwater routing and the Younger Dryas. *Proceedings of the National Academy of Sciences*, 109(49), 19928–19933. <https://doi.org/10.1073/pnas.1207381109>
- Cornish, S. B., Kostov, Y., Johnson, H. L., & Lique, C. (2020). Response of Arctic freshwater to the Arctic Oscillation in coupled climate models. *Journal of Climate*, 33(2020), 2533–2555. <https://doi.org/10.1175/jcli-d-19-0685.1>
- Cuny, J., Rhines, P. B., & Kwok, R. (2005). Davis Strait volume, freshwater and heat fluxes. *Deep Sea Research Part I: Oceanographic Research Papers*, 52(3), 519–542. <https://doi.org/10.1016/j.dsr.2004.10.006>
- Curry, B., Lee, C. M., Petrie, B., Moritz, R. E., & Kwok, R. (2014). Multiyear volume, liquid freshwater, and sea ice transports through Davis Strait, 2004–10. *Journal of Physical Oceanography*, 44(4), 1244–1266. <https://doi.org/10.1175/jpo-d-13-0177.1>
- Dee, D. P., Uppala, S. M., Simmons, A. J., Berrisford, P., Poli, P., Kobayashi, S., et al. (2011). The ERA-Interim reanalysis: Configuration and performance of the data assimilation system. *Quarterly Journal of the Royal Meteorological Society*, 137(656), 553–597. <https://doi.org/10.1002/qj.828>

Acknowledgments

Shizhu Wang was funded by the National Natural Science Foundation of China (Grant Nos. 42005044 and No. 41941012), and Postdoc Applied Research Foundation of Qingdao. Fangli Qiao was supported by the National Natural Science Foundation of China (Grant No. 41821004) and the Chinese National Program on Global Change and Air-Sea Interaction (GASI-IPOVAI-05). Qiang Wang was supported by the German Helmholtz Climate Initiative REKLIM (Regional Climate Change and Human) and the German Federal Ministry for Education and Research (BMBF) through the EPICA project (Grant No. 03F0889A). Muyin Wang was funded by the Joint Institute for the Study of the Atmosphere and Ocean (JISAO) (now Corporate Institute for Climate, Ocean, and Ecosystem Studies) under NOAA Cooperative Agreement NA15OAR4320063, Contribution No. 2020-1120, and NOAA MAPP grant NA19OAR4310286 to University of Washington. The Pacific Marine Environmental Laboratory contribution number is 5200 for this article. Gerrit Lohmann received funding from the programmes “Changing Earth-Sustaining our Future” and REKLIM through Helmholtz. The authors acknowledge all the groups for producing and providing their model, observation and/or reanalysis results.

- Dewey, S., Morison, J., Kwok, R., Dickinson, S., Morison, D., & Andersen, R. (2018). Arctic ice-ocean coupling and Gyre equilibration observed with remote sensing. *Geophysical Research Letters*, *45*(3), 1499–1508. <https://doi.org/10.1002/2017gl076229>
- Dukhovskoy, D. S., Johnson, M. A., & Proshutinsky, A. (2004). Arctic decadal variability: An auto-oscillatory system of heat and fresh water exchange. *Geophysical Research Letters*, *31*(3), 1–4. <https://doi.org/10.1029/2003GL019023>
- Eyring, V., Bony, S., Meehl, G. A., Senior, C. A., Stevens, B., Stouffer, R. J., & Taylor, K. E. (2016). *Overview of the coupled model Intercomparison project phase 6 (CMIP6) experimental design and organization* (p. 9). Geoscientific Model Development (Online). (LLNL-JRNL-736881).
- Fan, X., Duan, Q., Shen, C., Wu, Y., & Xing, C. (2020). Global surface air temperatures in CMIP6: Historical performance and future changes. *Environmental Research Letters*, *15*(10), 104056. <https://doi.org/10.1088/1748-9326/abb051>
- Feng, D., Gleason, C. J., Lin, P., Yang, X., Pan, M., & Ishitsuka, Y. (2021). Recent changes to Arctic river discharge. *Nature Communications*, *12*(1), 1–9. <https://doi.org/10.1038/s41467-021-27228-1>
- Fournier, S., Lee, T., Wang, X., Armitage, T. W. K., Wang, O., Fukumori, I., & Kwok, R. (2020). Sea surface salinity as a proxy for Arctic Ocean freshwater changes. *Journal of Geophysical Research: Oceans*, *125*. <https://doi.org/10.1029/2020jc016110>
- Fuentes-Franco, R., & Koenigk, T. (2019). Sensitivity of the Arctic freshwater content and transport to model resolution. *Climate Dynamics*, *53*(3–4), 1765–1781. <https://doi.org/10.1007/s00382-019-04735-y>
- Giles, K. A., Laxon, S. W., Ridout, A. L., Wingham, D. J., & Bacon, S. (2012). Western Arctic Ocean freshwater storage increased by wind-driven spin-up of the Beaufort Gyre. *Nature Geoscience*, *5*(3), 194–197. <https://doi.org/10.1038/ngeo1379>
- Gillett, N. P., Allen, M. R., McDonald, R. E., Senior, C. A., Shindell, D. T., & Schmidt, G. A. (2002). How linear is the Arctic Oscillation response to greenhouse gases? *Journal of Geophysical Research*, *107*(D3), 4022. <https://doi.org/10.1029/2001JD000589>
- Griffies, S. M., Danabasoglu, G., Durack, P. J., Adcroft, A. J., Balaji, V., Böning, C. W., et al. (2016). OMIP contribution to CMIP6: Experimental and diagnostic protocol for the physical component of the Ocean Model Intercomparison Project. *Geoscientific Model Development*, *9*(9), 3231–3296. <https://doi.org/10.5194/gmd-9-3231-2016>
- Guthrie, J. D., Morison, J. H., & Fer, I. (2013). Internal waves and mixing in the Arctic Ocean. *Deep-Sea Research Part A Oceanographic Research Papers*, *39*(8), 3966–3977. <https://doi.org/10.1002/jgrc.20294>
- Haine, T. W. N., Curry, B., Gerdes, R., Hansen, E., Karcher, M., Lee, C., et al. (2015). Arctic freshwater export: Status, mechanisms, and prospects. *Global and Planetary Change*, *125*, 13–35. <https://doi.org/10.1016/j.gloplacha.2014.11.013>
- Häkkinen, S. (1999). A simulation of thermohaline effects of a great salinity anomaly. *Journal of Climate*, *12*(6), 1781–1795. [https://doi.org/10.1175/1520-0442\(1999\)012<1781:asote>2.0.co;2](https://doi.org/10.1175/1520-0442(1999)012<1781:asote>2.0.co;2)
- Held, I. M., & Soden, B. J. (2006). Robust responses of the hydrological cycle to global warming. *Journal of Climate*, *19*(21), 5686–5699. <https://doi.org/10.1175/jcli3990.1>
- Holland, M. M., Finnis, J., Barrett, A. P., & Serreze, M. C. (2007). Projected changes in Arctic Ocean freshwater budgets. *Journal of Geophysical Research*, *112*(G4), G04S55. <https://doi.org/10.1029/2006jg000354>
- Holloway, G., & Proshutinsky, A. (2007). Role of tides in Arctic Ocean/ice climate. *Journal of Geophysical Research*, *112*(C4), C04S06. <https://doi.org/10.1029/2006jc003643>
- Holmes, R. M., McClelland, J. W., Peterson, B. J., Tank, S. E., Bulygina, E., Eglinton, T. I., et al. (2012). Seasonal and annual fluxes of nutrients and organic matter from large rivers to the Arctic Ocean and surrounding seas. *Estuaries and Coasts*, *35*(2), 369–382. <https://doi.org/10.1007/s12237-011-9386-6>
- Ilicak, M., Drange, H., Wang, Q., Gerdes, R., Aksenov, Y., Bailey, D., et al. (2016). An assessment of the Arctic Ocean in a suite of interannual CORE-II simulations. Part III: Hydrography and fluxes. *Ocean Modelling*, *100*, 141–161. <https://doi.org/10.1016/j.ocemod.2016.02.004>
- Jahn, A., Aksenov, Y., De Cuevas, B. A., De Steur, L., Häkkinen, S., Hansen, E., et al. (2012). Arctic Ocean freshwater: How robust are model simulations? *Journal of Geophysical Research*, *117*(C8), C00D16. <https://doi.org/10.1029/2012JC009707>
- Jahn, A., & Laiho, R. (2020). Forced changes in the Arctic freshwater budget emerge in the early 21st century. *Geophysical Research Letters*, *47*(15), e2020GL088854.
- Karcher, M. J., Gerdes, R., Kauker, F., Köberle, C., & Yashayaev, I. (2005). Arctic Ocean change heralds North Atlantic freshening. *Geophysical Research Letters*, *32*(21), 1–5. <https://doi.org/10.1029/2005GL023861>
- Khosravi, N., Wang, Q., Koldunov, N., Hinrichs, C., Semmler, T., Danilov, S., & Jung, T. (2022). The Arctic Ocean in CMIP6 models: Biases and projected changes in temperature and salinity. *Earth's Future*, *10*(2), e2021EF002282. <https://doi.org/10.1029/2021ef002282>
- Kipp, L. E., Charette, M. A., Moore, W. S., Henderson, P. B., & Rigor, I. G. (2018). Increased fluxes of shelf-derived materials to the central Arctic Ocean. *Science Advances*, *4*(1), eaao1302. <https://doi.org/10.1126/sciadv.aao1302>
- Krumpen, T., Gerdes, R., Haas, C., Hendricks, S., Herber, A., Selyuzhenok, V., et al. (2016). Recent Summer Sea ice thickness surveys in Fram Strait and associated ice volume fluxes. *The Cryosphere*, *10*(2), 523–534. <https://doi.org/10.5194/tc-10-523-2016>
- Kwok, R. (2018). Arctic sea ice thickness, volume, and multiyear ice coverage: Losses and coupled variability (1958–2018). *Environmental Research Letters*, *13*(10), 105005. <https://doi.org/10.1088/1748-9326/aae3ec>
- Landerer, F. W., Jungclauss, J. H., & Marotzke, J. (2007). Ocean bottom pressure changes lead to a decreasing length-of-day in a warming climate. *Geophysical Research Letters*, *34*(6), 1–5. <https://doi.org/10.1029/2006GL029106>
- Langehaug, H. R., Geyer, F., Smedsrud, L. H., & Gao, Y. (2013). Arctic sea ice decline and ice export in the CMIP5 historical simulations. *Ocean Modelling*, *71*, 114–126. <https://doi.org/10.1016/j.ocemod.2012.12.006>
- Lara, R. J., Rachold, V., Kattner, G., Hubberten, H. W., Guggenberger, G., Skoog, A., & Thomas, D. N. (1998). Dissolved organic matter and nutrients in the Lena river, Siberian Arctic: Characteristics and distribution. *Marine Chemistry*, *59*(3–4), 301–309. [https://doi.org/10.1016/S0304-4203\(97\)00076-5](https://doi.org/10.1016/S0304-4203(97)00076-5)
- Lind, S., Ingvaldsen, R. B., & Furevik, T. (2018). Arctic warming hotspot in the northern Barents Sea linked to declining sea-ice import. *Nature Climate Change*, *8*(7), 634–639. <https://doi.org/10.1038/s41558-018-0205-y>
- Luneva, M. V., Aksenov, Y., Harle, J. D., & Holt, J. T. (2015). The effects of tides on the water mass mixing and sea ice in the Arctic Ocean. *Journal of Geophysical Research: Oceans*, *120*(10), 6669–6699. <https://doi.org/10.1002/2014jc010310>
- Martinson, D. G., & Steele, M. (2001). Future of the Arctic sea ice cover: Implications of an Antarctic analog. *Geophysical Research Letters*, *28*(2), 307–310. <https://doi.org/10.1029/2000gl011549>
- McPhee, M. G., Proshutinsky, A., Morison, J. H., Steele, M., & Alkire, M. B. (2009). Rapid change in freshwater content of the Arctic Ocean. *Geophysical Research Letters*, *36*(10), L10602. <https://doi.org/10.1029/2009gl0137525>
- Meneghello, G., Marshall, J., Campin, J. M., Doddridge, E., & Timmermans, M. L. (2018). The Ice-Ocean governor: Ice-Ocean stress feedback limits Beaufort Gyre spin-up. *Geophysical Research Letters*, *45*(20), 11293–11299. <https://doi.org/10.1029/2018GL080171>
- Min, C., Yang, Q., Mu, L., Kauker, F., & Ricker, R. (2021). Ensemble-based estimation of sea-ice volume variations in the Baffin Bay. *The Cryosphere*, *15*(1), 169–181. <https://doi.org/10.5194/tc-15-169-2021>

- Min, S., Zhang, X., Zwiers, F. W., & Agnew, T. (2008). Human influence on Arctic sea ice detectable from early 1990s onwards. *Geophysical Research Letters*, 35(21), L21701. <https://doi.org/10.1029/2008gl035725>
- Morison, J., Kwok, R., Peralta-Ferriz, C., Alkire, M., Rigor, I., Andersen, R., & Steele, M. (2012). Changing Arctic Ocean freshwater pathways. *Nature*, 481(7379), 66–70. <https://doi.org/10.1038/nature10705>
- Münchow, A., Weingartner, T. J., & Cooper, L. W. (1999). The summer hydrography and surface circulation of the East Siberian Shelf Sea. *Journal of Physical Oceanography*, 29(9), 2167–2182. [https://doi.org/10.1175/1520-0485\(1999\)029<2167:tshasc>2.0.co;2](https://doi.org/10.1175/1520-0485(1999)029<2167:tshasc>2.0.co;2)
- Muntjewerf, L., Petrini, M., Vizcaino, M., Ernani da Silva, C., Sellevold, R., Scherrenberg, M. D. W., et al. (2020). Greenland ice sheet contribution to 21st century sea level rise as simulated by the coupled CESM2. 1-CISM2. 1. *Geophysical Research Letters*, 47(9), e2019GL086836. <https://doi.org/10.1029/2019gl086836>
- Niederdrenk, A. L., Sein, D. V., & Mikolajewicz, U. (2016). Interannual variability of the Arctic freshwater cycle in the second half of the twentieth century in a regionally coupled climate model. *Climate Dynamics*, 47(12), 3883–3900. <https://doi.org/10.1007/s00382-016-3047-1>
- Notz, D., & Stroeve, J. (2016). Observed Arctic sea-ice loss directly follows anthropogenic CO₂ emission. *Science*, 354(6313), 747–750. <https://doi.org/10.1126/science.aag2345>
- Nummelin, A., Ilicak, M., Li, C., & Smedsrud, L. H. (2016). Consequences of future increased Arctic runoff on Arctic Ocean stratification, circulation, and sea ice cover. *Journal of Geophysical Research: Oceans*, 121(1), 617–637. <https://doi.org/10.1002/2015jc011156>
- O'Neill, B. C., Tebaldi, C., Van Vuuren, D. P., Eyring, V., Friedlingstein, P., Hurtt, G., et al. (2016). The scenario model intercomparison project (ScenarioMIP) for CMIP6. *Geoscientific Model Development*, 9, 3461–3482. <https://doi.org/10.5194/gmd-9-3461-2016>
- Peterson, B. J., McClelland, J., Curry, R., Holmes, R. M., Walsh, J. E., & Aagaard, K. (2006). Trajectory shifts in the Arctic and subarctic freshwater cycle. *Science*, 313(5790), 1061–1066. <https://doi.org/10.1126/science.1122593>
- Pfirman, S. L., Colony, R., Nürnberg, D., Eicken, H., & Rigor, I. (1997). Reconstructing the origin and trajectory of drifting Arctic sea ice. *Journal of Geophysical Research*, 102(C6), 12575–12586. <https://doi.org/10.1029/96jc03980>
- Polyakov, I. V., Pnyushkov, A. V., Alkire, M. B., Ashik, I. M., Baumann, T. M., Carmack, E. C., et al. (2017). Greater role for Atlantic inflows on sea-ice loss in the Eurasian Basin of the Arctic Ocean. *Science*, 356(6335), 285–291. <https://doi.org/10.1126/science.aai8204>
- Polyakov, I. V., Pnyushkov, A. V., & Carmack, E. C. (2018). Stability of the arctic halocline: A new indicator of arctic climate change. *Environmental Research Letters*, 13(12), 125008. <https://doi.org/10.1088/1748-9326/aaec1e>
- Polyakov, I. V., Rippeth, T. P., Fer, I., Alkire, M. B., Baumann, T. M., Carmack, E. C., et al. (2020). Weakening of cold halocline layer exposes sea ice to oceanic heat in the eastern Arctic Ocean. *Journal of Climate*, 33(18), 8107–8123. <https://doi.org/10.1175/jcli-d-19-0976.1>
- Proshutinsky, A., Bourke, R. H., & McLaughlin, F. A. (2002). The role of the Beaufort Gyre in Arctic climate variability: Seasonal to decadal climate scales. *Geophysical Research Letters*, 29(23), 11–15. <https://doi.org/10.1029/2002gl015847>
- Proshutinsky, A., & Johnson, M. A. (1997). Two circulation regimes of the wind-driven Arctic Ocean. *Journal of Geophysical Research*, 102(C6), 12493–12514. <https://doi.org/10.1029/97JC00738>
- Proshutinsky, A., Krishfield, R., Toole, J., Timmermans, M., Williams, W., Zimmerman, S., et al. (2019). Analysis of the Beaufort Gyre freshwater content in 2003–2018. *Journal of Geophysical Research: Oceans*.
- Rabe, B., Karcher, M., Kauker, F., Schauer, U., Toole, J. M., Krishfield, R. A., et al. (2014). Arctic Ocean basin liquid freshwater storage trend 1992–2012. *Geophysical Research Letters*, 41(3), 961–968. <https://doi.org/10.1002/2013gl058121>
- Rigor, I. G., Wallace, J. M., & Colony, R. L. (2002). Response of sea ice to the Arctic Oscillation. *Journal of Climate*, 15(18), 2648–2663. [https://doi.org/10.1175/1520-0442\(2002\)015<2648:rositt>2.0.co;2](https://doi.org/10.1175/1520-0442(2002)015<2648:rositt>2.0.co;2)
- Roach, A. T., Aagaard, K., Pease, C. H., Salo, S. A., Weingartner, T., Pavlov, V., & Kulakov, M. (1995). Direct measurements of transport and water properties through the Bering Strait. *Journal of Geophysical Research*, 100(C9), 18443–18457. <https://doi.org/10.1029/95jc01673>
- Rosenblum, E., Fajber, R., Stroeve, J., Gille, S., Tremblay, B., & Carmack, E. (2021). Surface salinity under transitioning ice cover in the Canada Basin: Climate model biases linked to vertical 2 distribution of freshwater. *Geophysical Research Letters*, 48(21), e2021GL094739. <https://doi.org/10.1029/2021GL094739>
- Rudels, B., Anderson, L. G., & Jones, E. P. (1996). Formation and evolution of the surface mixed layer and halocline of the Arctic Ocean. *Journal of Geophysical Research*, 101(C4), 8807–8821. <https://doi.org/10.1029/96jc00143>
- Schauer, U., Beszczynska-Möller, A., Walczowski, W., Fahrbach, E., Piechura, J., & Hansen, E. (2008). Variation of measured heat flow through the Fram Strait between 1997 and 2006. In *Arctic-subarctic ocean fluxes* (pp. 65–85). Springer.
- Schweiger, A. J., Lindsay, R., Zhang, J., Steele, M., Stern, H., & Kwok, R. (2011). Uncertainty in modeled Arctic sea ice volume. *Journal of Geophysical Research*, 116(C8), C00D06. <https://doi.org/10.1029/2011jc007084>
- Schweiger, A. J., Wood, K. R., & Zhang, J. (2019). Arctic sea ice volume variability over 1901–2010: A model-based reconstruction. *Journal of Climate*, 32(15), 4731–4752. <https://doi.org/10.1175/JCLI-D-19-0008.1>
- Serreze, M. C., Barrett, A. P., Slater, A. G., Woodgate, R. A., Aagaard, K., Lammers, R. B., et al. (2006). The large-scale freshwater cycle of the Arctic. *Journal of Geophysical Research*, 111(C11), C11010. <https://doi.org/10.1029/2005jc003424>
- Shu, Q., Qiao, F., Song, Z., Zhao, J., & Li, X. (2018). Projected freshening of the Arctic Ocean in the 21st century. *Journal of Geophysical Research: Oceans*, 123(12), 9232–9244. <https://doi.org/10.1029/2018JC014036>
- Shu, Q., Song, Z., & Qiao, F. (2015). Assessment of sea ice simulations in the CMIP5 models. *The Cryosphere*, 9(1), 399–409. <https://doi.org/10.5194/tc-9-399-2015>
- Shu, Q., Wang, Q., Song, Z., Qiao, F., Zhao, J., Chu, M., & Li, X. (2020). Assessment of sea ice extent in CMIP6 with comparison to observations and CMIP5. *Geophysical Research Letters*, 47(9), e2020GL087965. <https://doi.org/10.1029/2020gl087965>
- SIMIP Community. (2020). Arctic sea ice in CMIP6. *Geophysical Research Letters*, 47(10), e2019GL086749. <https://doi.org/10.1029/2019gl086749>
- Skagseth, Ø., Furevik, T., Ingvaldsen, R., Loeng, H., Mork, K. A., Orvik, K. A., & Ozhigin, V. (2008). Volume and heat transports to the Arctic Ocean via the Norwegian and Barents seas. In *Arctic-subarctic ocean fluxes* (pp. 45–64). Springer.
- Smedsrud, L. H., Esau, I., Ingvaldsen, R. B., Eldevik, T., Haugan, P. M., Li, C., et al. (2013). The role of the Barents Sea in the Arctic climate system. *Reviews of Geophysics*, 51(3), 415–449. <https://doi.org/10.1002/rog.20017>
- Smedsrud, L. H., Ingvaldsen, R., Nilsen, J. E. Ø., & Skagseth, Ø. (2010). Heat in the Barents Sea: Transport, storage, and surface fluxes. *Ocean Science*, 6(1), 219–234. <https://doi.org/10.5194/os-6-219-2010>
- Spall, M. A. (2019). Dynamics and thermodynamics of the mean transpolar drift and ice thickness in the Arctic Ocean. *Journal of Climate*, 32(24), 8449–8463. <https://doi.org/10.1175/JCLI-D-19-0252.1>
- Spall, M. A. (2020). Potential vorticity dynamics of the Arctic Halocline. *Journal of Physical Oceanography*, 50(9), 2491–2506. <https://doi.org/10.1175/jpo-d-20-0056.1>
- Spren, G., de Steur, L., Divine, D., Gerland, S., Hansen, E., & Kwok, R. (2020). Arctic sea ice volume export through Fram Strait from 1992 to 2014. *Journal of Geophysical Research: Oceans*, 125(6), e2019JC016039. <https://doi.org/10.1029/2019jc016039>

- Steele, M., & Boyd, T. (1998). Retreat of the cold halocline layer in the Arctic Ocean. *Journal of Geophysical Research*, *103*(C5), 10419–10435. <https://doi.org/10.1029/98jc00580>
- Steele, M., & Ermold, W. (2004). Salinity trends on the Siberian shelves. *Geophysical Research Letters*, *31*(24), L24308. <https://doi.org/10.1029/2004gl021302>
- Steele, M., Morley, R., & Ermold, W. (2001). PHC: A global ocean hydrography with a high-quality Arctic Ocean. *Journal of Climate*, *14*(9), 2079–2087. [https://doi.org/10.1175/1520-0442\(2001\)014<2079:pagoHW>2.0.CO;2](https://doi.org/10.1175/1520-0442(2001)014<2079:pagoHW>2.0.CO;2)
- Stöven, T., Tanhua, T., Hoppema, M., & von Appen, W.-J. (2016). Transient tracer distributions in the Fram Strait in 2012 and inferred anthropogenic carbon content and transport. *Ocean Science*, *12*(1), 319–333. <https://doi.org/10.5194/os-12-319-2016>
- Stroeve, J., & Notz, D. (2018). Changing state of Arctic sea ice across all seasons. *Environmental Research Letters*, *13*(10), 103001. <https://doi.org/10.1088/1748-9326/aade56>
- Tebaldi, C., Ranasinghe, R., Voudoukas, M., Rasmussen, D. J., Vega-westhoff, B., Kirezci, E., et al. (2021). Extreme sea levels at different global warming levels. *Nature Climate Change*, *11*, 746–751. <https://doi.org/10.1038/s41558-021-01127-1>
- Thornalley, D. J. R., Oppo, D. W., Ortega, P., Robson, J. I., Brierley, C. M., Davis, R., et al. (2018). Anomalously weak Labrador Sea convection and Atlantic overturning during the past 150 years. *Nature*, *556*(7700), 227–230. <https://doi.org/10.1038/s41586-018-0007-4>
- Timmermans, M., Proshutinsky, A., Krishfield, R. A., Perovich, D. K., Richter-Menge, J. A., Stanton, T. P., & Toole, J. M. (2011). Surface freshening in the Arctic Ocean's Eurasian Basin: An apparent consequence of recent change in the wind-driven circulation. *Journal of Geophysical Research*, *116*(C8), C00D03. <https://doi.org/10.1029/2011jc006975>
- Tokarska, K. B., Stolpe, M. B., Sippel, S., Fischer, E. M., Smith, C. J., Lehner, F., & Knutti, R. (2020). Past warming trend constrains future warming in CMIP6 models. *Science Advances*, *6*(12), 1–14. <https://doi.org/10.1126/sciadv.aaz9549>
- Vavrus, S. J., Holland, M. M., Jahn, A., Bailey, D. A., & Blazey, B. A. (2012). Twenty-first-century Arctic climate change in CCSM4. *Journal of Climate*, *25*(8), 2696–2710. <https://doi.org/10.1175/jcli-d-11-00220.1>
- Wang, Q., Danilov, S., Sidorenko, D., & Wang, X. (2021). Circulation pathways and exports of Arctic river runoff influenced by atmospheric circulation regimes. *Frontiers in Marine Science*, *8*, 707593. <https://doi.org/10.3389/fmars.2021.707593>
- Wang, Q., Ilicak, M., Gerdes, R., Drange, H., Aksenov, Y., Bailey, D. A., et al. (2016a). An assessment of the Arctic Ocean in a suite of interannual CORE-II simulations. Part I: Sea ice and solid freshwater. *Ocean Modelling*, *99*, 86–109. <https://doi.org/10.1016/j.ocemod.2015.12.009>
- Wang, Q., Ilicak, M., Gerdes, R., Drange, H., Aksenov, Y., Bailey, D. A., et al. (2016b). An assessment of the Arctic Ocean in a suite of interannual CORE-II simulations. Part II: Liquid freshwater. *Ocean Modelling*, *99*, 86–109. <https://doi.org/10.1016/j.ocemod.2015.12.009>
- Wang, Q., Marshall, J., Scott, J., Meneghello, G., Danilov, S., & Jung, T. (2019). On the feedback of Ice-Ocean stress coupling from geostrophic currents in an anticyclonic wind regime over the Beaufort Gyre. *Journal of Physical Oceanography*, *49*(2), 369–383. <https://doi.org/10.1175/jpo-d-18-0185.1>
- Wang, Q., Ricker, R., & Mu, L. (2021). Arctic sea ice decline preconditions events of anomalously low sea ice volume export through Fram Strait in the early 21st century. *Journal of Geophysical Research: Oceans*, *126*(2), 1–14. <https://doi.org/10.1029/2020jc016607>
- Wang, Q., Shu, Q., Danilov, S., & Sidorenko, D. (2022). An extreme event of enhanced Arctic Ocean export west of Greenland caused by the pronounced dynamic sea level drop in the North Atlantic subpolar gyre in the mid-to-late 2010s. *Environmental Research Letters*, *17*(4), 044046. <https://doi.org/10.1088/1748-9326/ac5562>
- Wang, Q., Wekerle, C., Danilov, S., Koldunov, N., Sidorenko, D., Sein, D., et al. (2018). Arctic sea ice decline significantly contributed to the unprecedented liquid freshwater accumulation in the Beaufort Gyre of the Arctic Ocean. *Geophysical Research Letters*, *45*(10), 4956–4964. <https://doi.org/10.1029/2018GL077901>
- Wang, Q., Wekerle, C., Danilov, S., Sidorenko, D., Koldunov, N., Sein, D., et al. (2019). Recent sea ice decline did not significantly increase the total liquid freshwater content of the Arctic Ocean. *Journal of Climate*, *32*(1), 15–32. <https://doi.org/10.1175/JCLI-D-18-0237.1>
- Wang, Q., Wekerle, C., Danilov, S., Wang, X., & Jung, T. (2018). A 4.5 km resolution Arctic Ocean simulation with the global multi-resolution model FESOM 1.4. *Geoscientific Model Development*, *11*(4), 1229–1255. <https://doi.org/10.5194/gmd-11-1229-2018>
- Wang, Q., Wekerle, C., Wang, X., Danilov, S., Koldunov, N., Sein, D., et al. (2020). Intensification of the Atlantic water supply to the Arctic Ocean through Fram Strait induced by Arctic Sea Ice decline. *Geophysical Research Letters*, *47*(3). <https://doi.org/10.1029/2019GL086682>
- Wang, S., Wang, Q., Shu, Q., Song, Z., Lohmann, G., Danilov, S., & Qiao, F. (2021). Nonmonotonic change of the Arctic Ocean freshwater storage capability in a warming climate. *Geophysical Research Letters*, *48*(10), e2020GL090951. <https://doi.org/10.1029/2020gl090951>
- Woodgate, R. A. (2018). Increases in the Pacific inflow to the Arctic from 1990 to 2015, and insights into seasonal trends and driving mechanisms from year-round Bering Strait mooring data. *Progress in Oceanography*, *160*, 124–154. <https://doi.org/10.1016/j.pocean.2017.12.007>
- Yin, J., Griffies, S. M., & Stouffer, R. J. (2010). Spatial variability of sea level rise in twenty-first century projections. *Journal of Climate*, *23*(17), 4585–4607. <https://doi.org/10.1175/2010JCLI3533.1>
- Yin, J. H. (2005). A consistent poleward shift of the storm tracks in simulations of 21st century climate. *Geophysical Research Letters*, *32*(18). <https://doi.org/10.1029/2005gl023684>
- Zanowski, H., Jahn, A., & Holland, M. M. (2021). Arctic Ocean freshwater in cmip6 ensembles: Declining sea ice, increasing ocean storage and export. *Journal of Geophysical Research: Oceans*, *126*(4), e2020JC016930. <https://doi.org/10.1029/2020jc016930>
- Zhang, J., & Rothrock, D. A. (2003). Modeling global sea ice with a thickness and enthalpy distribution model in generalized curvilinear coordinates. *Monthly Weather Review*, *131*(5), 845–861. [https://doi.org/10.1175/1520-0493\(2003\)131<0845:mgsiwa>2.0.CO;2](https://doi.org/10.1175/1520-0493(2003)131<0845:mgsiwa>2.0.CO;2)
- Zhang, J., & Steele, M. (2007). Effect of vertical mixing on the Atlantic water layer circulation in the Arctic Ocean. *Journal of Geophysical Research*, *112*(C4), C04S04. <https://doi.org/10.1029/2006jc003732>
- Zhang, J., Steele, M., Runciman, K., Dewey, S., Morison, J., Lee, C., et al. (2016). The Beaufort Gyre intensification and stabilization: A model-observation synthesis. *Journal of Geophysical Research: Oceans*, *121*(11), 7933–7952. <https://doi.org/10.1002/2016JC012196>
- Zhang, X., He, J., Zhang, J., Polyakov, I., Gerdes, R., Inoue, J., & Wu, P. (2013). Enhanced poleward moisture transport and amplified northern high-latitude wetting trend. *Nature Climate Change*, *3*(1), 47–51. <https://doi.org/10.1038/nclimate1631>
- Zuo, H., Balmaseda, M. A., Tietsche, S., Mogensen, K., & Mayer, M. (2019). The ECMWF operational ensemble reanalysis–analysis system for Ocean and sea ice: A description of the system and assessment. *Ocean Science*, *15*(3), 779–808. <https://doi.org/10.5194/os-15-779-2019>

References From the Supporting Information

- Bentsen, M., Olivière, D. J. L., Seland, Ø., Toniazzo, T., Gjermundsen, A., Graff, L. S., et al. (2019a). NCC NorESM2-MM model output prepared for CMIP6 CMIP historical. Version 20191129. *Earth System Grid Federation*. <https://doi.org/10.22033/ESGF/CMIP6.8040>
- Bentsen, M., Olivière, D. J. L., Seland, Ø., Toniazzo, T., Gjermundsen, A., Graff, L. S., et al. (2019b). NCC NorESM2-MM model output prepared for CMIP6 ScenarioMIP ssp245. Version 20200210. *Earth System Grid Federation*. <https://doi.org/10.22033/ESGF/CMIP6.8255>

- Bentsen, M., Oliv  , D. J. L., Seland,  ., Toniazzo, T., Gjermundsen, A., Graff, L. S., et al. (2019c). NCC NorESM2-MM model output prepared for CMIP6 ScenarioMIP ssp585. Version 20200131. *Earth System Grid Federation*. <https://doi.org/10.22033/ESGF/CMIP6.8321>
- Boucher, O., Denvil, S., Levavasseur, G., Cozic, A., Caubel, A., Foujols, M.-A., et al. (2018). IPSL IPSL-CM6A-LR model output prepared for CMIP6 CMIP historical. Version 20180731. *Earth System Grid Federation*. <https://doi.org/10.22033/ESGF/CMIP6.5195>
- Boucher, O., Denvil, S., Levavasseur, G., Cozic, A., Caubel, A., Foujols, M.-A., et al. (2019a). IPSL IPSL-CM6A-LR model output prepared for CMIP6 ScenarioMIP ssp245. Version 20181205. *Earth System Grid Federation*. <https://doi.org/10.22033/ESGF/CMIP6.5264>
- Boucher, O., Denvil, S., Levavasseur, G., Cozic, A., Caubel, A., Foujols, M.-A., et al. (2019b). IPSL IPSL-CM6A-LR model output prepared for CMIP6 ScenarioMIP ssp585. Version 20181218. *Earth System Grid Federation*. <https://doi.org/10.22033/ESGF/CMIP6.5271>
- Cao, J. (2019a). NUIST NESMv3 model output prepared for CMIP6 ScenarioMIP ssp245. Version 20190731. *Earth System Grid Federation*. <https://doi.org/10.22033/ESGF/CMIP6.8781>
- Cao, J. (2019b). NUIST NESMv3 model output prepared for CMIP6 ScenarioMIP ssp585. Version 20190730. *Earth System Grid Federation*. <https://doi.org/10.22033/ESGF/CMIP6.8790>
- Cao, J., & Wang, B. (2019). NUIST NESMv3 model output prepared for CMIP6 CMIP historical. Version 20190703. *Earth System Grid Federation*. <https://doi.org/10.22033/ESGF/CMIP6.8769>
- Danabasoglu, G. (2019a). NCAR CESM2 model output prepared for CMIP6 CMIP historical. Version 20190402. *Earth System Grid Federation*. <https://doi.org/10.22033/ESGF/CMIP6.7627>
- Danabasoglu, G. (2019b). NCAR CESM2 model output prepared for CMIP6 ScenarioMIP ssp245. Version 20200526. *Earth System Grid Federation*. <https://doi.org/10.22033/ESGF/CMIP6.7748>
- Danabasoglu, G. (2019c). NCAR CESM2 model output prepared for CMIP6 ScenarioMIP ssp585. Version 20200526. *Earth System Grid Federation*. <https://doi.org/10.22033/ESGF/CMIP6.7768>
- Danabasoglu, G. (2019d). NCAR CESM2-WACCM model output prepared for CMIP6 CMIP historical. Version 20190729. *Earth System Grid Federation*. <https://doi.org/10.22033/ESGF/CMIP6.10071>
- Danabasoglu, G. (2019e). NCAR CESM2-WACCM model output prepared for CMIP6 ScenarioMIP ssp245. Version 20190331. *Earth System Grid Federation*. <https://doi.org/10.22033/ESGF/CMIP6.10101>
- Danabasoglu, G. (2019f). NCAR CESM2-WACCM model output prepared for CMIP6 ScenarioMIP ssp585. Version 20190208. *Earth System Grid Federation*. <https://doi.org/10.22033/ESGF/CMIP6.10115>
- Dix, M., Bi, D., Dobrohotoff, P., Fiedler, R., Harman, I., Law, R., et al. (2019a). CSIRO-ARCCSS ACCESS-CM2 model output prepared for CMIP6 CMIP historical. Version 20191108. *Earth System Grid Federation*. <https://doi.org/10.22033/ESGF/CMIP6.4271>
- Dix, M., Bi, D., Dobrohotoff, P., Fiedler, R., Harman, I., Law, R., et al. (2019b). CSIRO-ARCCSS ACCESS-CM2 model output prepared for CMIP6 ScenarioMIP ssp245. Version 20191108. *Earth System Grid Federation*. <https://doi.org/10.22033/ESGF/CMIP6.4321>
- Dix, M., Bi, D., Dobrohotoff, P., Fiedler, R., Harman, I., Law, R., et al. (2019c). CSIRO-ARCCSS ACCESS-CM2 model output prepared for CMIP6 ScenarioMIP ssp585. Version 20191108. *Earth System Grid Federation*. <https://doi.org/10.22033/ESGF/CMIP6.4332>
- EC-Earth Consortium (EC-Earth). (2019a). EC-Earth-Consortium EC-Earth3-Veg model output prepared for CMIP6 CMIP historical. Version 20190610. *Earth System Grid Federation*. <https://doi.org/10.22033/ESGF/CMIP6.4706>
- EC-Earth Consortium (EC-Earth). (2019b). EC-Earth-Consortium EC-Earth3-Veg model output prepared for CMIP6 ScenarioMIP ssp245. Version 20190629. *Earth System Grid Federation*. <https://doi.org/10.22033/ESGF/CMIP6.4882>
- EC-Earth Consortium (EC-Earth). (2019c). EC-Earth-Consortium EC-Earth3-Veg model output prepared for CMIP6 ScenarioMIP ssp585. Version 20190630. *Earth System Grid Federation*. <https://doi.org/10.22033/ESGF/CMIP6.4914>
- EC-Earth Consortium (EC-Earth). (2019d). EC-Earth-Consortium EC-Earth3 model output prepared for CMIP6 CMIP historical. Version 20190926. *Earth System Grid Federation*. <https://doi.org/10.22033/ESGF/CMIP6.4700>
- EC-Earth Consortium (EC-Earth). (2019e). EC-Earth-Consortium EC-Earth3 model output prepared for CMIP6 ScenarioMIP ssp245. Version 20190927. *Earth System Grid Federation*. <https://doi.org/10.22033/ESGF/CMIP6.4880>
- EC-Earth Consortium (EC-Earth). (2019f). EC-Earth-Consortium EC-Earth3 model output prepared for CMIP6 ScenarioMIP ssp585. Version 20190928. *Earth System Grid Federation*. <https://doi.org/10.22033/ESGF/CMIP6.4912>
- Good, P. (2019). MOHC HadGEM3-GC31-LL model output prepared for CMIP6 ScenarioMIP ssp245. Version 20190418. *Earth System Grid Federation*. <https://doi.org/10.22033/ESGF/CMIP6.10851>
- Good, P. (2020). MOHC HadGEM3-GC31-LL model output prepared for CMIP6 ScenarioMIP ssp585. Version 20190724. *Earth System Grid Federation*. <https://doi.org/10.22033/ESGF/CMIP6.10901>
- Good, P., Sellar, A., Tang, Y., Rumbold, S., Ellis, R., Kelley, D., & Kuhlbrodt, T. (2019a). MOHC UKESM1.0-LL model output prepared for CMIP6 ScenarioMIP ssp245. Version 20190906. *Earth System Grid Federation*. <https://doi.org/10.22033/ESGF/CMIP6.6339>
- Good, P., Sellar, A., Tang, Y., Rumbold, S., Ellis, R., Kelley, D., & Kuhlbrodt, T. (2019b). MOHC UKESM1.0-LL model output prepared for CMIP6 ScenarioMIP ssp585. Version 20200113. *Earth System Grid Federation*. <https://doi.org/10.22033/ESGF/CMIP6.6405>
- Guo, H., John, J. G., Blanton, C., McHugh, C., Nikonov, S., Radhakrishnan, A., et al. (2018a). NOAA-GFDL GFDL-CM4 model output historical. Version 20190223. *Earth System Grid Federation*. <https://doi.org/10.22033/ESGF/CMIP6.8594>
- Guo, H., John, J. G., Blanton, C., McHugh, C., Nikonov, S., Radhakrishnan, A., et al. (2018b). NOAA-GFDL GFDL-CM4 model output prepared for CMIP6 ScenarioMIP ssp245. Version 20190318. *Earth System Grid Federation*. <https://doi.org/10.22033/ESGF/CMIP6.9263>
- Guo, H., John, J. G., Blanton, C., McHugh, C., Nikonov, S., Radhakrishnan, A., et al. (2018c). NOAA-GFDL GFDL-CM4 model output prepared for CMIP6 ScenarioMIP ssp585. Version 20190320. *Earth System Grid Federation*. <https://doi.org/10.22033/ESGF/CMIP6.9268>
- Huang, W. (2019). THU CIESM model output prepared for CMIP6 CMIP historical. Version 20191231. *Earth System Grid Federation*. <https://doi.org/10.22033/ESGF/CMIP6.8843>
- Huang, W. (2020a). THU CIESM model output prepared for CMIP6 ScenarioMIP ssp245. Version 20200323. *Earth System Grid Federation*. <https://doi.org/10.22033/ESGF/CMIP6.8858>
- Huang, W. (2020b). THU CIESM model output prepared for CMIP6 ScenarioMIP ssp585. Version 20191231. *Earth System Grid Federation*. <https://doi.org/10.22033/ESGF/CMIP6.8863>
- John, J. G., Blanton, C., McHugh, C., Radhakrishnan, A., Rand, K., Vahlenkamp, H., et al. (2018a). NOAA-GFDL GFDL-ESM4 model output prepared for CMIP6 ScenarioMIP ssp245. Version 20190619. *Earth System Grid Federation*. <https://doi.org/10.22033/ESGF/CMIP6.8686>
- John, J. G., Blanton, C., McHugh, C., Radhakrishnan, A., Rand, K., Vahlenkamp, H., et al. (2018b). NOAA-GFDL GFDL-ESM4 model output prepared for CMIP6 ScenarioMIP ssp585. Version 20190618. *Earth System Grid Federation*. <https://doi.org/10.22033/ESGF/CMIP6.8706>
- Jungclaus, J., Bittner, M., Wieners, K.-H., Wachsmann, F., Schupfner, M., Legutke, S., et al. (2019). MPI-M MPI-ESM1.2-HR model output prepared for CMIP6 CMIP historical. Version 20190825. *Earth System Grid Federation*. <https://doi.org/10.22033/ESGF/CMIP6.6594>
- Krasting, J. P., John, J. G., Blanton, C., McHugh, C., Nikonov, S., Radhakrishnan, A., et al. (2018). NOAA-GFDL GFDL-ESM4 model output prepared for CMIP6 CMIP historical. Version 20190806. *Earth System Grid Federation*. <https://doi.org/10.22033/ESGF/CMIP6.8597>

- Li, L. (2019a). CAS FGOALS-g3 model output prepared for CMIP6 CMIP historical. Version 20191012. *Earth System Grid Federation*. <https://doi.org/10.22033/ESGF/CMIP6.3356>
- Li, L. (2019b). CAS FGOALS-g3 model output prepared for CMIP6 ScenarioMIP ssp245. Version 20191231. *Earth System Grid Federation*. <https://doi.org/10.22033/ESGF/CMIP6.3469>
- Li, L. (2019c). CAS FGOALS-g3 model output prepared for CMIP6 ScenarioMIP ssp585. Version 20191230. *Earth System Grid Federation*. <https://doi.org/10.22033/ESGF/CMIP6.3503>
- Lovato, T., & Peano, D. (2020a). CMCC CMCC-CM2-SR5 model output prepared for CMIP6 CMIP historical. Version 20200528. *Earth System Grid Federation*. <https://doi.org/10.22033/ESGF/CMIP6.3825>
- Lovato, T., & Peano, D. (2020b). CMCC CMCC-CM2-SR5 model output prepared for CMIP6 ScenarioMIP ssp245. Version 20200615. *Earth System Grid Federation*. <https://doi.org/10.22033/ESGF/CMIP6.3889>
- Lovato, T., & Peano, D. (2020c). CMCC CMCC-CM2-SR5 model output prepared for CMIP6 ScenarioMIP ssp585. Version 20200616. *Earth System Grid Federation*. <https://doi.org/10.22033/ESGF/CMIP6.3896>
- NASA Goddard Institute for Space Studies (NASA/GISS). (2018). NASA-GISS GISS-E2.1G model output prepared for CMIP6 CMIP historical. Version 20190819. *Earth System Grid Federation*. <https://doi.org/10.22033/ESGF/CMIP6.7127>
- NASA Goddard Institute for Space Studies (NASA/GISS). (2020a). NASA-GISS GISS-E2.1G model output prepared for CMIP6 ScenarioMIP ssp245. Version 20200206. *Earth System Grid Federation*. <https://doi.org/10.22033/ESGF/CMIP6.7415>
- NASA Goddard Institute for Space Studies (NASA/GISS). (2020b). NASA-GISS GISS-E2.1G model output prepared for CMIP6 ScenarioMIP ssp585. Version 20200208. *Earth System Grid Federation*. <https://doi.org/10.22033/ESGF/CMIP6.7460>
- Ridley, J., Menary, M., Kuhlbrodt, T., Andrews, M., & Andrews, T. (2019). MOHC HadGEM3-GC31-LL model output prepared for CMIP6 CMIP historical. Version 20190619. *Earth System Grid Federation*. <https://doi.org/10.22033/ESGF/CMIP6.6109>
- Rong, X. (2019a). CAMS CAMS-CSM1.0 model output prepared for CMIP6 CMIP historical. Version 20190703. *Earth System Grid Federation*. <https://doi.org/10.22033/ESGF/CMIP6.9754>
- Rong, X. (2019b). CAMS CAMS-CSM1.0 model output prepared for CMIP6 ScenarioMIP ssp245. Version 20190702. *Earth System Grid Federation*. <https://doi.org/10.22033/ESGF/CMIP6.11047>
- Rong, X. (2019c). CAMS CAMS-CSM1.0 model output prepared for CMIP6 ScenarioMIP ssp585. Version 20190702. *Earth System Grid Federation*. <https://doi.org/10.22033/ESGF/CMIP6.11052>
- Schupfner, M., Wieners, K.-H., Wachsmann, F., Steger, C., Bittner, M., Jungclaus, J., et al. (2019a). DKRZ MPI-ESM1.2-HR model output prepared for CMIP6 ScenarioMIP ssp245. Version 20190722. *Earth System Grid Federation*. <https://doi.org/10.22033/ESGF/CMIP6.4398>
- Schupfner, M., Wieners, K.-H., Wachsmann, F., Steger, C., Bittner, M., Jungclaus, J., et al. (2019b). DKRZ MPI-ESM1.2-HR model output prepared for CMIP6 ScenarioMIP ssp585. Version 20190723. *Earth System Grid Federation*. <https://doi.org/10.22033/ESGF/CMIP6.4403>
- Seferian, R. (2018). CNRM-CERFACS CNRM-ESM2-1 model output prepared for CMIP6 CMIP historical. Version 20181009. *Earth System Grid Federation*. <https://doi.org/10.22033/ESGF/CMIP6.4068>
- Seland, Ø., Bentsen, M., Olivie, D. J. L., Toniazzo, T., Gjermundsen, A., Graff, L. S., et al. (2019a). NCC NorESM2-LM model output prepared for CMIP6 CMIP historical. Version 20190815. *Earth System Grid Federation*. <https://doi.org/10.22033/ESGF/CMIP6.8036>
- Seland, Ø., Bentsen, M., Olivie, D. J. L., Toniazzo, T., Gjermundsen, A., Graff, L. S., et al. (2019b). NCC NorESM2-LM model output prepared for CMIP6 ScenarioMIP ssp245. Version 20191208. *Earth System Grid Federation*. <https://doi.org/10.22033/ESGF/CMIP6.8253>
- Seland, Ø., Bentsen, M., Olivie, D. J. L., Toniazzo, T., Gjermundsen, A., Graff, L. S., et al. (2019c). NCC NorESM2-LM model output prepared for CMIP6 ScenarioMIP ssp585. Version 20191221. *Earth System Grid Federation*. <https://doi.org/10.22033/ESGF/CMIP6.8319>
- Semmler, T., Danilov, S., Rackow, T., Sidorenko, D., Barbi, D., Hegewald, J., et al. (2018a). AWI AWI-CM1.1MR model output prepared for CMIP6 CMIP historical. Version 20181218. *Earth System Grid Federation*. <https://doi.org/10.22033/ESGF/CMIP6.2686>
- Semmler, T., Danilov, S., Rackow, T., Sidorenko, D., Barbi, D., Hegewald, J., et al. (2018b). AWI AWI-CM1.1MR model output prepared for CMIP6 ScenarioMIP ssp245. Version 20181218. *Earth System Grid Federation*. <https://doi.org/10.22033/ESGF/CMIP6.2800>
- Semmler, T., Danilov, S., Rackow, T., Sidorenko, D., Barbi, D., Hegewald, J., et al. (2019). AWI AWI-CM1.1MR model output prepared for CMIP6 ScenarioMIP ssp585. Version 20181218. *Earth System Grid Federation*. <https://doi.org/10.22033/ESGF/CMIP6.2817>
- Song, Z., Qiao, F., Bao, Y., Shu, Q., Song, Y., & Yang, X. (2019a). FIO-QLNM FIO-ESM2.0 model output prepared for CMIP6 CMIP historical. Version 20191209. *Earth System Grid Federation*. <https://doi.org/10.22033/ESGF/CMIP6.9199>
- Song, Z., Qiao, F., Bao, Y., Shu, Q., Song, Y., & Yang, X. (2019b). FIO-QLNM FIO-ESM2.0 model output prepared for CMIP6 ScenarioMIP ssp245. Version 20200109. *Earth System Grid Federation*. <https://doi.org/10.22033/ESGF/CMIP6.9209>
- Song, Z., Qiao, F., Bao, Y., Shu, Q., Song, Y., & Yang, X. (2019c). FIO-QLNM FIO-ESM2.0 model output prepared for CMIP6 ScenarioMIP ssp585. Version 20200114. *Earth System Grid Federation*. <https://doi.org/10.22033/ESGF/CMIP6.9214>
- Swart, N. C., Cole, J. N. S., Kharin, V. V., Lazare, M., Scinocca, J. F., Gillett, N. P., et al. (2019a). CCCma CanESM5 model output prepared for CMIP6 CMIP historical. Version 20190429. *Earth System Grid Federation*. <https://doi.org/10.22033/ESGF/CMIP6.3610>
- Swart, N. C., Cole, J. N. S., Kharin, V. V., Lazare, M., Scinocca, J. F., Gillett, N. P., et al. (2019b). CCCma CanESM5 model output prepared for CMIP6 ScenarioMIP ssp245. Version 20190429. *Earth System Grid Federation*. <https://doi.org/10.22033/ESGF/CMIP6.3685>
- Swart, N. C., Cole, J. N. S., Kharin, V. V., Lazare, M., Scinocca, J. F., Gillett, N. P., et al. (2019c). CCCma CanESM5 model output prepared for CMIP6 ScenarioMIP ssp585. Version 20190429. *Earth System Grid Federation*. <https://doi.org/10.22033/ESGF/CMIP6.3696>
- Swart, N. C., Cole, J. N. S., Kharin, V. V., Lazare, M., Scinocca, J. F., Gillett, N. P., et al. (2019d). CCCma CanESM5-CanOE model output prepared for CMIP6 CMIP historical. Version 20190429. *Earth System Grid Federation*. <https://doi.org/10.22033/ESGF/CMIP6.10260>
- Swart, N. C., Cole, J. N. S., Kharin, V. V., Lazare, M., Scinocca, J. F., Gillett, N. P., et al. (2019e). CCCma CanESM5-CanOE model output prepared for CMIP6 ScenarioMIP ssp245. Version 20190429. *Earth System Grid Federation*. <https://doi.org/10.22033/ESGF/CMIP6.10270>
- Swart, N. C., Cole, J. N. S., Kharin, V. V., Lazare, M., Scinocca, J. F., Gillett, N. P., et al. (2019f). CCCma CanESM5-CanOE model output prepared for CMIP6 ScenarioMIP ssp585. Version 20190429. *Earth System Grid Federation*. <https://doi.org/10.22033/ESGF/CMIP6.10276>
- Tang, Y., Rumbold, S., Ellis, R., Kelley, D., Mulcahy, J., Sellar, A., et al. (2019). MOHC UKESM1.0-LL model output prepared for CMIP6 CMIP historical. Version 20190624. *Earth System Grid Federation*. <https://doi.org/10.22033/ESGF/CMIP6.6113>
- Voltaire, A. (2018). CMIP6 simulations of the CNRM-CERFACS based on CNRM-CM6-1 model for CMIP experiment historical. Version 20180713. *Earth System Grid Federation*. <https://doi.org/10.22033/ESGF/CMIP6.4066>
- Voltaire, A. (2019a). CNRM-CERFACS CNRM-CM6-1 model output prepared for CMIP6 ScenarioMIP ssp245. Version 20181122. *Earth System Grid Federation*. <https://doi.org/10.22033/ESGF/CMIP6.4189>
- Voltaire, A. (2019b). CNRM-CERFACS CNRM-CM6-1 model output prepared for CMIP6 ScenarioMIP ssp585. Version 20181125. *Earth System Grid Federation*. <https://doi.org/10.22033/ESGF/CMIP6.4224>
- Voltaire, A. (2019c). CNRM-CERFACS CNRM-CM6-1-HR model output prepared for CMIP6 CMIP historical. Version 20190729. *Earth System Grid Federation*. <https://doi.org/10.22033/ESGF/CMIP6.4067>

- Voldoire, A. (2019d). CNRM-CERFACS CNRM-CM6-1-HR model output prepared for CMIP6 ScenarioMIP ssp245. Version 20191112. *Earth System Grid Federation*. <https://doi.org/10.22033/ESGF/CMIP6.4190>
- Voldoire, A. (2019e). CNRM-CERFACS CNRM-CM6-1-HR model output prepared for CMIP6 ScenarioMIP ssp585. Version 20191027. *Earth System Grid Federation*. <https://doi.org/10.22033/ESGF/CMIP6.4225>
- Voldoire, A. (2019f). CNRM-CERFACS CNRM-ESM2-1 model output prepared for CMIP6 ScenarioMIP ssp245. Version 20180828. *Earth System Grid Federation*. <https://doi.org/10.22033/ESGF/CMIP6.4191>
- Voldoire, A. (2019g). CNRM-CERFACS CNRM-ESM2-1 model output prepared for CMIP6 ScenarioMIP ssp585. Version 20180828. *Earth System Grid Federation*. <https://doi.org/10.22033/ESGF/CMIP6.4226>
- Volodin, E., Mortikov, E., Gritsun, A., Lykossov, V., Galin, V., Diansky, N., et al. (2019a). INM INM-CM5-0 model output prepared for CMIP6 CMIP historical. Version 20190607. *Earth System Grid Federation*. <https://doi.org/10.22033/ESGF/CMIP6.5070>
- Volodin, E., Mortikov, E., Gritsun, A., Lykossov, V., Galin, V., Diansky, N., et al. (2019b). INM INM-CM5-0 model output prepared for CMIP6 ScenarioMIP ssp245. Version 20190619. *Earth System Grid Federation*. <https://doi.org/10.22033/ESGF/CMIP6.12328>
- Volodin, E., Mortikov, E., Gritsun, A., Lykossov, V., Galin, V., Diansky, N., et al. (2019c). INM INM-CM5-0 model output prepared for CMIP6 ScenarioMIP ssp585. Version 20190724. *Earth System Grid Federation*. <https://doi.org/10.22033/ESGF/CMIP6.12338>
- Wieners, K.-H., Giorgetta, M., Jungclaus, J., Reick, C., Esch, M., Bittner, M., et al. (2019a). MPI-M MPI-ESM1.2-LR model output prepared for CMIP6 CMIP historical. Version 20190904. *Earth System Grid Federation*. <https://doi.org/10.22033/ESGF/CMIP6.6595>
- Wieners, K.-H., Giorgetta, M., Jungclaus, J., Reick, C., Esch, M., Bittner, M., et al. (2019b). MPI-M MPI-ESM1.2-LR model output prepared for CMIP6 ScenarioMIP ssp245. Version 20191105. *Earth System Grid Federation*. <https://doi.org/10.22033/ESGF/CMIP6.6693>
- Wieners, K.-H., Giorgetta, M., Jungclaus, J., Reick, C., Esch, M., Bittner, M., et al. (2019c). MPI-M MPI-ESM1.2-LR model output prepared for CMIP6 ScenarioMIP ssp585. Version 20191112. *Earth System Grid Federation*.
- Wu, T., Chu, M., Dong, M., Fang, Y., Jie, W., Li, J., et al. (2018). BCC BCC-CSM2MR model output prepared for CMIP6 CMIP historical. Version 20181126. *Earth System Grid Federation*. <https://doi.org/10.22033/ESGF/CMIP6.2948>
- Xin, X., Wu, T., Shi, X., Zhang, F., Li, J., Chu, M., et al. (2019a). BCC BCC-CSM2MR model output prepared for CMIP6 ScenarioMIP ssp245. Version 20190319. *Earth System Grid Federation*. <https://doi.org/10.22033/ESGF/CMIP6.3030>
- Xin, X., Wu, T., Shi, X., Zhang, F., Li, J., Chu, M., et al. (2019b). BCC BCC-CSM2MR model output prepared for CMIP6 ScenarioMIP ssp585. Version 20190319. *Earth System Grid Federation*. <https://doi.org/10.22033/ESGF/CMIP6.3050>
- Yukimoto, S., Koshiro, T., Kawai, H., Oshima, N., Yoshida, K., Urakawa, S., et al. (2019a). MRI MRI-ESM2.0 model output prepared for CMIP6 CMIP historical. Version 20191114. *Earth System Grid Federation*. <https://doi.org/10.22033/ESGF/CMIP6.6842>
- Yukimoto, S., Koshiro, T., Kawai, H., Oshima, N., Yoshida, K., Urakawa, S., et al. (2019b). MRI MRI-ESM2.0 model output prepared for CMIP6 ScenarioMIP ssp245. Version 20191210. *Earth System Grid Federation*. <https://doi.org/10.22033/ESGF/CMIP6.6910>
- Yukimoto, S., Koshiro, T., Kawai, H., Oshima, N., Yoshida, K., Urakawa, S., et al. (2019c). MRI MRI-ESM2.0 model output prepared for CMIP6 ScenarioMIP ssp585. Version 20191209. *Earth System Grid Federation*. <https://doi.org/10.22033/ESGF/CMIP6.6929>
- Ziehn, T., Chamberlain, M., Lenton, A., Law, R., Bodman, R., Dix, M., et al. (2019a). CSIRO ACCESS-ESM1.5 model output prepared for CMIP6 CMIP historical. Version 20191115. *Earth System Grid Federation*. <https://doi.org/10.22033/ESGF/CMIP6.4272>
- Ziehn, T., Chamberlain, M., Lenton, A., Law, R., Bodman, R., Dix, M., et al. (2019b). CSIRO ACCESS-ESM1.5 model output prepared for CMIP6 ScenarioMIP ssp245. Version 20191115. *Earth System Grid Federation*. <https://doi.org/10.22033/ESGF/CMIP6.4322>
- Ziehn, T., Chamberlain, M., Lenton, A., Law, R., Bodman, R., Dix, M., et al. (2019c). CSIRO ACCESS-ESM1.5 model output prepared for CMIP6 ScenarioMIP ssp585. Version 20191108. *Earth System Grid Federation*. <https://doi.org/10.22033/ESGF/CMIP6.4333>